Dear Prof. Macedonio,

We have uploaded the revised version of the manuscript. Our response to the comments by A. Folch and M. Herzog as well as a marked-up manuscript are attached to our cover letter below. We have tried to incorporate most of the comments and suggestions by both reviewers. Details are given below in the detailed response.

The most relevant changes made in the manuscript are:

- We revised some of the figures to better show the different ash isosurfaces and to use more consistent colorbars (see Fig. 2 - 6, 11)
- We significantly extended the model description part (p. 3 and 4)

Furthermore several minor changes have been made to the manuscript in order to increase precision and clarity.

We would like to thank you, both reviewers as well as all persons involved in processing this manuscript and we honestly hope that you find our revisions of the manuscript sufficient and look forward to hear from you.

Kind regards

Elena Gerwing

Authors reply to comments by A. Folch[1]

1. *The model does not take into account for processes known to be relevant in ash cloud dynamics such as diffusion, dry/wet deposition mechanisms or ash aggregation. As a result, the model cloud dynamics limits to wind advection and particle sedimentation. Near-source effects (e.g. plume dynamics or gravity current) are ignored. On the other hand and more important, I do not understand why particle ground deposition is not contemplated. A part from the obvious interest of estimating ash/tephra fallout, the computation of the deposit is necessary (together with satellite imagery) for model validation (see below)*

   Indeed the model is simplified with respect to the ash cloud chemistry and microphysical processes. Our focus in this paper lies exclusively on the adaptive mesh methodology together with the simulation of sedimentation in context of the Lagrangian approach. Therefore processes like wet/dry deposition and ash aggregation are not considered. In order to consider plume dynamics and gravity currents other models like Atham or PDAC are certainly more appropriate to do so. After all, this is only an advective model like the basic Fall3D but with the add on of an adaptive mesh. Therefore we only focused on gravitational sedimentation further away from the plume stem.

   We have added one sentence into the introduction that we neglect this process as this is not the focus of the paper (p. 2, lines 31-33)

   The quantification of sedimentation to the ground (fall-out) could certainly be included but is at the moment not implemented in the model.

   Long term goal of our work is to include adaptive meshing into models like ATHAM or PDAC or any general GCM model. We consider this study as a first feasibility study for this endeavor and hope to encourage more scientists to work along these lines.

   We have added an extra paragraph at the end of the manuscript describing our roadmap for further developments (p. 21, lines 6-11)

2. *The innovative aspect of this manuscript is the use of adaptive grids in ash cloud simulations. However, several aspects regarding the numerical algorithm and its advantages are not detailed. Is the mesher embedded in the code? How often is the refinement applied? At each time integration step or at user-defined time intervals? The overhead of performing variable interpolation after each refinement and weather this is done in a conservative way or not is not mentioned.*

   You are right, we omitted these important aspects. But we will add this information in a revised version.
   The model uses a quasi-conservative semi-Lagrangian approach, as documented in (Behrens, 2006). This is a low order upstream interpolation method that can handle complex flow fields in 3D yet is simple enough not to impose too strict computational demands. The mesh refinement is triggered, as defined by the refinement criterion. As indicated in the manuscript, the tolerance for refinement is set to 0.02, which means that a grid cell is marked for refinement if the ash concentration gradient of the cell is above 2 percent of the maximum of all concentration gradients. The refinement criterion is calculated during each time step, but the actual refinement takes place only, if sufficiently many cells are marked for refinement. In our model at least 0.1 percent of the cells need to be marked for refinement to perform the refinement of the grid. The semi-Lagrangian scheme requires an interpolation in each step.

   The section describing the model has been significantly extended to incorporate the questions addressed by A. Folch (p. 3 and 4)

3. *The authors conclude that (pg 18, lines 1-4): "we have demonstrated the versatility of adaptive meshing algorithms for modeling the dispersion of volcanic emissions. Especially the high performance*

[1] Note that all references with pages and line numbers refer to the annotated manuscript.

of this code would allow, if implemented into operational ash dispersion models, a significant improvement of dispersion predictions as model runs could be carried out significantly faster compared to codes using a fixed grid". Certainly there is a potential, but I think that this conclusion is too precipitated for many reasons. Constraining to Eulerian models (where this assertion would make sense), an important point not mentioned is code parallelism (most operational models actually run in parallel). The drawbacks of mesh adaptivity in the parallel execution of transient (time-evolving) problems are well-known: redefine the optimal domain decomposition at each refinement to ensure processor load balance has large associated interpolation and communication costs, code scalability breaks, etc. As a result, it is unclear whether the strategy would suppose a gain or not when running on hundreds of processors. This affects the main conclusion of this manuscript.

While it is true that our simulations were carried out in serial mode, the code has also shown parallel efficiency (Behrens et al., 2005) and recently even more effective ways of parallelization have been presented (Behrens and Bader, 2009), all compatible with our algorithm. So, the authors do not see a general problem with parallelizing the code efficiently. The main message here is that even without a large parallel infrastructure, one can perform reasonably highly resolved simulations with just a laptop. We briefly mentioned in the manuscript the possibility of using the code in parallel.

Nothing has been changed in the manuscript to address this issue. We note that even in the org. manuscript we mentioned that the code could be executed in parallel (p. 2, line 22).

4. *Another controversial aspect which is not discussed by the authors is that "we apply the model for individual particle diameters and then combine the results of different runs to predict the sedimentation of the complete grain size distribution", pg. 4, line 22). I understand that this is necessary because the different particle sizes require of different refinements. However, how this affects efficiency in case on several (e.g. 10) particle classes is not even mentioned. Is the comparison shown in Figure 12 for a single class? This may not be fair, but it is difficult for a reader to extract conclusions since no details are given on the fraction of computation time of remeshing/interpolation. I suggest comparing the time of 10 simulations (coarse 8, fine 17) with that of a single run with all 10 classes and fixed grid.*

Currently the sedimentation of the particles is calculated by adding a vertical wind component to the wind field that is equivalent to settling velocity of that respective particle size. In principle the code could be rewritten to include an array of tracers of different size, each of which is advected with its individual wind field. The refinement criterion would then be applied to all tracer concentrations via the maximum gradient considering all tracers such that all tracers are well resolved.

We have added a comment on this in the conclusions (p. 20, lines 10 - 13).

5. *I missed details on the model numerical algorithm. Is it explicit or implicit? What about the time integration step (only 10 min is mentioned in pg. 4 line 17, but based on what?).*

The authors do not understand this remark. We use a semi-Lagrangian scheme. For the advection equation, this states that the upstream value of a material density needs to be preserved along trajectories. This in an unconditionally stable scheme.
Now, the conservative scheme does not only consider material particles, but cells, which may be distorted due to shear, convergence, divergence in the flow field. This imposes a stability restriction, since the cells are not allowed to degenerate in one time step. But under mild conditions on the regularity of the flow field this still gives a stable scheme. Therefore the time step is relatively irrelevant and given here for information only.

See the extended section on the model (p. 3 and 4).

6. *Model validation could certainly be improved. I wonder why the Pinatubo eruption was selected to this purpose given some obvious difficulties: the role of the gravity current (see Costa et al., Geophysical Research Letters, vol. 40, 1–5, doi:10.1002/grl.50942, 2013), the particular meteorological conditions at that time, the lack of extensive deposit sampling and inferred TGSD, etc. In any case, some quantitative model validation would be worth. On the other hand, it is stated (e.g. Table 4) that the refinement level goes down to <5 km. However, it seems that the driving meteorology is at 55 km and the wind field is linearly interpolated. Does it make sense? My impression is that refinement at sharp concentration gradients helps because it reduces numerical diffusion…*

   We accept the criticism that more model validation could be done. However, since this study is mainly of methodological character and since we used a very simplified chemistry, we decided to focus on a more qualitative approach.
   Regarding to the mesh refinement beyond the given wind field. This has been addressed in a former study (Behrens et al (2000)), were we showed that even in a very smooth/homogeneous flow field high resolution may be beneficial if shear in the flow field leads to stirring. So, we argue that even if the wind field does not contain small scale features, the transport benefits from high resolution. And yes, one of the effects that helps in this situation is the reduced numerical diffusion from high resolution.

   Nothing has been changed in the manuscript to address this issue.

7. *Sensitivity study (section 4.1). The effect of variation in initial cloud height is actually a combined effect of injection height and driving meteorology (REMOTE)…*

   We do not really understand, what the reviewer wants to express with this remark. Of course is this a combination of injection height with the wind field, and the simulated dispersion is a result of the prevailing wind conditions in the prescribed vertical layers of the injection.

   As we were not clear about this comment nothing has been changed in the manuscript.

Specific comments

We corrected the minor issues directly in the manuscript. A revised version will be uploaded following the Editors decision.

Pg. 2, line 16. Parenthesis in reference

Done!

Pg 2, line 26. "very low computational cost". This is too vague and generic: : :Also, values of "seconds" is not what Fig. 12 shows.

In Fig. 12 we actually compare one run with an adaptive mesh with calculations on a uniform mesh. Clearly the adaptive mesh with the same refinement level as the calculation on a uniform mesh is 10 times faster. Admittedly it still takes close to an hour so we rewrote the sentence accordingly.

Has been rewritten (p. 2, lines 26/27)

Pg. 3, lines 8-9. The resolution of 0.5x0.5 is that of REMOTE? If so, I do not understand which is the gain with respect to driving global ECMWF (Era-Interim?) data, already available at this resolution. Do you mean that the mesoscale simulation is not used to increase the wind field resolution?

We used model results from a mesoscale model instead of meteorological analysis data, as they offer more flexibility for potential future applications, such as higher temporal resolution, e.g. in one hour intervals, increased spatial resolution, e.g. up to 10 km (Langmann et al., 2009), and model output for processes not yet included, such as rain rate per layer for wet deposition.

Nothing has been changed.

Pg. 3, line 12. Parenthesis in reference

Done!

Pg. 3, line 12. Like?

We did not really understand this remark.

Pg. 3., line 15. Model ! Domain

Has been changed.

Pg. 3, equations (1) and (3). Even if only advection is considered, shouldn't these equations include the terms C(div_u) (where u = u_REMOTE+u_t)? Is the wind from REMOTE divergence free? Can the z-gradient of the terminal settling velocity be ignored?

We are not sure what the reviewer is referring to. The advection equation is applied to the particle concentration (see eq. 1 and 3), i.e. the divergence of the particle concentration field needs to be known at this point not the divergence of the velocity field, as would be the case if we solve for the Navier Stokes equation that includes the divergence of the wind velocity field.

This section has been rewritten and we hope this clarifies the issue (p. 3).

Pg. 4, line 26: "Since this work is a first case study of the modeling of sedimentation of ash particles on an adaptive mesh the impact of rain on the sedimentation and aggregation of ash particles is neglected." This is ok, but I have concerns about how aggregation could ever be incorporated in a future using this strategy. With sedimentation each particle class has to have its own mesh (different model runs) and aggregation requires concurrency.

We are certainly aware of this problem and in this version of the code this is not possible. See also answer to remark 4 above.

We made a comment at the end of the conclusion on how to incorporate sedimentation of multiple particle classes in one single run.

Pg. 5, lines 12-13. Are hours correct?

Yes, three hours after the onset of the climactic eruption (at 13:40) the intensity began to decline at 16:40 and nine hours after the onset (at 22:40) the climactic eruption phase ended.

Nothing has been changed.

Pg. 6, line 5: "This atypical wind in the lower and middle troposphere caused the wide distribution of tephra in nearly all directions around the volcano". Was this a meteo effect or because the radial gravity current?

We assume that it is mainly a meteorological effect (compare Wolfe and Hoblitt, 1996).

Nothing has been changed.

Pg. 8, Table 4. The horizontal/vertical element aspect ratio seems very large for tetrahedral elements (_100). Any hint on mesh element quality? In case of small angle, can this lead to oscillations/convergence problems?

Indeed the vertical vs. horizontal spatial scales are very distinct and the mesh quality in this respect is low. However, in the presented model, the mesh is used for interpolation and for maintaining conservation properties. For this type of application the mesh quality is of minor importance. Additionally, the non-uniform/anisotropic mesh supports the anisotropy in atmospheric scales (vertical vs. horizontal velocity ratio for example).

Nothing has been changed.

Pg. 9, line 15. "concentration on the surface". What does it mean? Which value? How is this defined?

As indicated by the colorbar, the surface of the cloud is supposed to have an ash concentration of 1x10^(-3) kg/m^3. Of course this value is quite arbitrary, but we had to pick one value.

We added a describing sentence to each figure caption displaying the ash concentration on isosurfaces.

Figure 7 (and others). Why so many contours of observations? Only the corresponding to the time should be shown for clarity.

We will fix the coloring of the contours in a revised version of the manuscript.

We marked the relevant contour line in red, see Fig. 7.

References cited above

J. Behrens (2006). Adaptive Atmospheric Modeling - Key Techniques in Grid Generation, Data Structures, and Numerical Operations with Applications. Lecture Notes in Computational Science and Engineering, 54, Springer Verlag, Berlin, Heidelberg.

J. Behrens, N. Rakowsky, W. Hiller, D. Handorf, M. Läuter, J. Päpke, K. Dethloff (2005). amatos: Parallel Adaptive Mesh Generator for Atmospheric and Oceanic Simulation, Ocean Modelling, 12(1-2):171-183.

J. Behrens and M. Bader (2009): Efficiency Considerations in Triangular Adaptive Mesh Refinement, Phil. Trans. R. Soc. A, 367:4577-4589, DOI:10.1098/rsta.2009.0175.

J. Behrens, K. Dethloff, W. Hiller, A. Rinke (2000). Evolution of Small-Scale Filaments in an Adaptive Advection Model for Idealized Tracer Transport. Mon. Wea. Rev., 128:2976-2982.

Langmann, B., M. Hort and T. Hansteen, Meteorological influence on seasonal and diurnal variability of Nicaraguan volcanic emission dispersion: A numerical model study, J. Volc. Geotherm. Res. 182, 34–44, 2009

Wolfe, E. W. and Hoblitt, R. P.: Overview of the Eruptions, Quezon City : Philippine Institute of Volcanology and Seismology ; Seattle : University of Washington Press, http://pubs.usgs.gov/pinatubo/wolfe/index.html, 1996.

Authors Reply to comments by M. Herzog

1. *The biggest issue is the model initialization and forcing. It is said (page 7, line 6-8) that the initial concentration is derived by dividing the eruption rate by the injection volume. However, this results in a flux of ash mass per unit volume and time, not a concentration. This flux should have been maintained over the duration of the corresponding eruption phase. However, it seems that an initial perturbation/concentration was used instead. If this is true, then this is a major flaw of the paper. Only adding the ash emitted within one second underestimates the erupted ash mass by many orders of magnitude. Releasing all ash erupted during each phase (as listed in table 1) instantaneously at the beginning of an eruption phase is equally unrealistic. This issue needs to be addressed, simulations repeated if needed before the manuscript can be published.*

   Also, the total amount of ash should not depend on the choice of the grid. If the forced volume is different, then the ash flux into that volume should be (slightly) different to compensate.

   The emitted ash per eruption rate was neither released instantaneously at the beginning of the eruption nor was only the ash amount emitted during one second introduced per time step. The calculated mass eruption rates in kg/s (listed in Table 1 in the manuscript) were divided by the injection volume and multiplied by the simulation time step, ending up in an ash concentration in kg/m^3. Since this process wasn't described in the manuscript, we will add a short explanation in order to avoid confusion.

   We added a sentence in order to clarify the procedure (p. 8, lines 8 – 10).

   Since the injection volume was approximated better or worse by the adaptive mesh dependent on the refinement level, it is true that the total injected amount of ash slightly differs for the different grid resolutions. But these differences are quite small. In the grid configuration used for most of the simulations (an adaptive mesh with a fine grid level of 17 and a coarse grid level of 8) as well as for a uniform mesh with a refinement level of 17, about 99.5 % of the calculated mass was included in the initial cloud area, while the uniform grid with a refinement level of 14 still comprised 97.6 % of the original mass.

   Compare page 9, lines 16 – 18.

2. *In the abstract (page 1, line 3) and conclusions (page 18, line 5) the authors state that adaptive meshes are useful to resolve filament structures of volcanic emissions. However, in the chosen example and in the presented results no filaments are present. The authors need to better justify and motivate the selection of the Pinatubo eruption as a case study.*

   The reviewer is right in observing no fine filamentation in the experiment data. The Mount Pinatubo case was selected due to available data sets both in wind fields and initial conditions (injection rates) and coverage data. The argument of filamentation was used due to earlier experience with similar but fictional simulations (e.g. Behrens et al. 2000).

   Nothing has been changed.

3. *The model description (chapter 2) does not describe the semi-Lagrangian transport model in any detail. The reference (Behrens, 1996) is given but it is not clear from the text that the transport model is described in there. More details at least about the model concept are needed with a proper reference to the Behrens (1996) paper for further details.*

   While the authors did not feel that gap in the description and decided to omit such technical details for better readability and brevity, we are happy to add some more detail on the implementation and algorithmic details in a revised version of the paper (see also our comments on the review of A. Folch).

This part has been substantially rewritten (see pages 3 and 4).

4. *Add in the last paragraph of page 4 that ash is treated as a passive tracer. Particle deposition (page 4, line 28) was not monitored. It is unclear why, when it would have been as easy to implement as suggested in the conclusions (page 18, line 14-15). Since deposited ash is the main source of information for historical eruptions it would have been good to test the resolution dependence of that deposition.*

   The treatment as a passive tracer has be added to the revised manuscript. (p. 6 line 11)

   It is certainly true that more model validation – especially the evaluation of particle deposition – could be done. It is, however, technically quite complicated because of the mesh changing over time, which is the reason for omitting it at this point. As already explained when replying to the review of A. Folch the main purpose of this paper is to focus on the adaptive mesh methodology applied to the simulation of ash advection and sedimentation and not on the exact reproduction of a specific volcanic eruption.

   Nothing has been changed in this regard.

5. *The mass eruption rate in table 1 has wrong units. I would assume it is kg per second instead.*

   We changed it to kg/s.

6. *In table 2 add 'refinement' to the word level to avoid confusion with vertical levels.*

   Done.

7. *A cloud radius in degrees is an odd choice since this means an elliptical shape in physical space. This is inconsistent with the stated initial radial expansion of the plume on page 5. Discuss and clarify.*

   Since the simulation grid is in degree, we decided to define the initial radius in degrees as well; and with an initial radius of only three degree the shape only deviates from a perfect circle by a few kilometers, which is below the highest resolution of the model.

   But for very explosive volcanic eruptions with an initial radius exceeding a few degrees, or for studies with a very high vertical resolution, it should be considered to define the initial radius in kilometers.

   Nothing has been changed in this regard.

8. *I disagree that results are converged for fine mesh levels larger than 16 (page 9, line1-2). According to figure 3, ash concentrations in the centre of the plume to the south west of the volcano increase significantly from fine mesh levels 17 to 20 and to 23.Quantify the differences and discuss convergence or non-convergence in greater detail.*

   The problem with convergence is that it can only be tested for smooth and therefore idealized data. So, we decided to address the convergence issue not in detail but to focus on qualitatively similar results at different refinement levels. What is meant is the fact that from refinement level 17 onward, qualitative differences between the levels are very minor. Based on this observation we decided to run most of the experiments on this refinement level.

   Nothing has been changed in this regard.

Other minor issues:

We corrected the minor issues directly in the manuscript. A revised version will be uploaded following the Editors decision.

Page 1, line 17: fall out of tephra

Done!

Page 1, line 18: tephra fall(s) out can lead…

Done!

Page 2, line 2-3: add: …warmer winters and colder summer on the Northern hemisphere continents through dynamical feedbacks and radiative forcing, respectively (Robock, 2000).

Done!

Page 2, line 4-6: timescales of minutes don't influence the diurnal cycle

It is written that tephra is remaining in the atmosphere on timescales of minutes to weeks, which influences the diurnal cycle.

Nothing has been changed.

Page 5, line 3: remove 'one of' since it has been said before that Pinatubo was the largest eruption in the 20th century.

No, it was not stated before, that the Pinatubo eruption was the largest during the 20th century. In fact according to the Smithsonian Catalogue the largest eruption of the 20th century was the Novarupta eruption of 1912, the Pinatubo eruption was the largest eruption in terms of stratospheric disturbances.

Nothing has been changed.

Page 6, line 5: what is 'atypical' about the winds?

Not corresponding to the prevailing southwest wind owing to the passing typhoon (compare Wolfe and Hoblitt, 1996).

Added explanation in manuscript.

Page 7, line 20: say already here that 7 times means refinement level 8 (in table 2).Write 'in the initial model domain before refinement'.

Corrected.

Page 10, figure 3: increase font of colour bar and text.

Done.

Page 11, figure 4: use identical and more meaningful colour bar. There are no yellow or red colours visible. What defines the surface of the ash cloud? If it is a threshold concentration the figure should show an iso-surface. Explain.

This and following comments refer to the colorbars of the figures. This was also noted by the other reviewer A. Folch.

Figures have been updated.

Page 12, figure 5: use same colour bar for both panels to enable comparison.

See above, last comment.

Page 12, line 15: delete 'however'.

Done.

Page 12, line 11-17: use information from table 3 for superposition of different ash sizes. Ideally, this should give the best fit and allow for a more independent validation.

The authors are not sure what the reviewer suggests: Should we use all different particle sizes simultaneously and superposition the different results for the different percentages of their respective contribution?

Our aim was to show the influence of using different particle sizes on the reproduction of the climactic eruption cloud. Obviosly, the best correspondence with observations would be obtained by using all measured particle classes with their corresponding percentage.

Nothing has been changed.

Page 13, figure 6: use identical and more meaningful colour bars. Yellow and red colours not visible.

See comment above.

Page 15, line 16: 'since none of our (model) simulations'

Done!

Page 16, line 3-4: write: will (not might) be underestimated

Done!

Page 17, line 5-7 and page 18, figure 11: it is not obvious to me that the shape is recovered well in all calculations. Quantify differences, in particular, discuss differences between top right and bottom right panels (identical fine resolution). Label for bottom right panel: shouldn't it read 'coarse=8'?

Figure 11 and description has been revised.

Page 17, line 8-12: this is the common way to calculate performance gains due to adaptation. However, a transport model written and optimized for constant resolution can be significantly faster than an adaptive grid code run at constant grid resolution. Discuss to which extend this issue might apply here.

We assume that the performance of the semi-Lagrangian method employed here is relatively independent of the mesh design. Since we use a specialized algorithmic design that is based on a gather-scatter mechanism (see Behrens et al. 2005) for the ability to perform numerical operations on stride-one-vectors rather than unstructured meshes, earlier experiments have shown that the overhead imposed due to the adaptive mesh refinement is below some 5 % of the total run-time.

Nothing has been changed as we consider this too technical to be incorporated into the manuscript.

Page 17, line 12: unresolved reference

Has been fixed.

References

J. Behrens, N. Rakowsky, W. Hiller, D. Handorf, M. Läuter, J. Päpke, K. Dethloff (2005). amatos: Parallel Adaptive Mesh Generator for Atmospheric and Oceanic Simulation, Ocean Modelling, 12(1-2):171-183.

J. Behrens, K. Dethloff, W. Hiller, A. Rinke (2000). Evolution of Small-Scale Filaments in an Adaptive Advection Model for Idealized Tracer Transport. Mon. Wea. Rev., 128:2976-2982.

Wolfe, E. W. and Hoblitt, R. P (1996). Overview of the Eruptions. Quezon City : Philippine Institute of Volcanology and Seismology ; Seattle : University of Washington Press, http://pubs.usgs.gov/pinatubo/wolfe/index.html.

An Adaptive Semi-Lagrangian Advection Model for Transport of Volcanic Emissions in the Atmosphere

Elena Gerwing[1,a], Matthias Hort[1], Jörn Behrens[2], and Bärbel Langmann[1]

[1]Institute of Geophysics, University Hamburg, Bundesstr. 55, 20146 Hamburg, Germany
[2]Department of Mathematics, Differential Equations and Dynamical Systems, Bundesstr. 55, 20146 Hamburg, Germany
[a]now at: Alfred Wegener Institute, Helmholtz Centre for Polar and Marine Research, Am Handelshafen 12, 27570 Bremerhaven, Germany

Correspondence to: Elena Gerwing (elena.gerwing@uni-hamburg.de)

Abstract. Dispersion of volcanic emissions in the Earth atmosphere is of interest for climate research, air traffic control as well as human wellbeing. Current volcanic emission dispersion models rely on fixed grid structures that often are not able to resolve the fine filamented structure of volcanic emissions while being transported in the atmosphere. Here we extend an existing adaptive semi-Lagrangian advection model for volcanic emissions including the sedimentation of volcanic ash. The advection of volcanic emissions is driven by a pre-calculated wind field. For evaluation of the model, the explosive eruption of Mount Pinatubo in June 1991 is chosen, which was one of the largest eruptions in the 20th Century. We compare our simulations of the climactic eruption on June 15, 1991 to satellite data of the Pinatubo ash cloud and evaluate different sets of input parameters. We could reproduce the general advection of the Pinatubo ash cloud and owing to the adaptive mesh, simulations could be performed at a high local resolution while minimizing computational cost. Differences to the observed ash cloud are attributed to uncertainties in the input parameters and the pass by of Typhoon Yunya, which is probably not completely resolved in the wind data used to drive the model. Best results were achieved for simulations with multiple ash particle sizes.

1 Introduction

Tephra and SO_2 emissions from large volcanic eruptions have a crucial impact on short- and long-term climate variations, air traffic and the living conditions of people in the surrounding of volcanoes. Large tropical and high-latitude eruptions were primary drivers of interannual-to-decadal temperature changes in the Northern Hemisphere during the last 2500 years (e.g., Sigl et al., 2015). However, even smaller volcanic eruptions do significantly affect the living conditions on a local scale. For example, the respiration of volcanic ash and gas (e.g., Horwell and Baxter, 2006) is along with the fall out of tephra (e.g., Paladio-Melosantos et al., 1996) the most important impact on the local scale. Heavy tephra ~~falls~~ fall can lead to collapse of buildings, destruction of mechanical and electrical systems, disruption of transport systems, formation of enormous lahars, chemical and physical changes in water quality and damage of vegetation, crops, forestry and pastures (Folch, 2012). Drifting ash clouds pose a serious thread to jet aircraft and can lead to engine failure (e.g., FOUNDATION, 1993). Since 1976 an average number of two damaging encounters per year between aircraft and ash clouds has been reported (Ken Salazar, 2010),

and Clarkson et al. (2016) lately reviewed available engine and volcanological data and proposed a new 'Safe-to-Fly' chart with a much lower ash concentration threshold than previously recommended.

Volcanic SO_2 injected into the stratosphere has a global impact by its conversion to sulphate aerosol which disturbs the Earth's radiation balance. Tropical volcanic eruptions thereby lead to warmer winters and colder summers on the Northern ~~Hemisphere continents~~ hemisphere continents through dynamical feedbacks and radiative forcing, respectively (Robock, 2000). In addition, volcanic aerosols lead to an increase in stratospheric particle surface area, enhancing the ozone destruction especially in high latitudes (Solomon, 1999). The amplitude of the diurnal cycle of the surface air temperature is reduced by volcanic tephra remaining in the atmosphere on timescales from minutes to weeks (Robock, 2000).

In order to mitigate risks and assess hazards originating from volcanic clouds, accurate observations and forecasts are needed. Advecting volcanic clouds can be tracked by satellite observations, but satellite images in the visible spectrum only result in outer contours of the cloud. Moreover, the global coverage and image frequency of satellite observations is highly inhomogeneous and satellite images only reflect the current state and can not be used for forecasting. Therefore, numerical models predicting the advection of ash or SO_2 are necessary.

There are several models simulating the advection (and sedimentation) of ash and SO_2 clouds. They are mainly performed on a regular grid and can generally be divided into two types by their numerical framework: *Eulerian models* like ATHAM (Oberhuber et al., 1998), REMOTE (Langmann, 2000), Fall3d (Folch et al., 2009) or Ash3d (Schwaiger et al., 2012) and *Lagrangian models* including Puff (Searcy et al., 1998) and NAME III (Jones et al., 2007). Additionally, there are some models using other approaches like semi-analytical tephra transport and dispersion models ~~(~~ HAZMAP (Macedonio et al., 2005; Pfeiffer et al., 2005) or TEPHRA (Bonadonna et al., 2005) ~~)~~ and the Lagrangian-Eularian model Vol-CALPUFF (Barsotti et al., 2008) and a volcanological adaptation of HySplit (Stein et al., 2015). For more details on these models the reader is referred to a recent review by Folch (2012).

In this article, we extend an existing semi-Lagrangian advection model performed on an adaptive, triangulated mesh (*Amatos* and *Flash*: Behrens (1996); Behrens et al. (2000)) for volcanic emissions. The semi-Lagrangian method has the advantage of a very stable and numerically efficient advection calculation and can be performed in parallel (Behrens, 1996). Adaptive mesh methods have the additional advantage of high resolution in the area where the advected cloud currently resides, while the computational cost is kept relatively low by using a coarse mesh ~~ouside~~ outside the cloud. With this model, simulations forecasting the advection of an ash cloud for several days could be performed at ~~very~~ low computational cost (CPU times of ~~seconds to minutes)~~ less than one hour) in contrast to comparable simulations on an uniform mesh which needed about nine times longer. We apply our new model to the advection and sedimentation of tephra, because SO_2 clouds cover a much larger area and the sedimentation of tephra occurs in timescales of minutes to weeks, while SO_2 and sulphate can remain in the atmosphere for some years. We concentrate on the advection of the ash cloud, neglecting complex eruption column dynamics and the influence of the eruption column on the surrounding atmosphere. This is a valid assumption, because far enough from the vent, these effects play a minor role (Folch, 2012). Furthermore we note that our model neglects processes like ash aggregation as well as wet and dry deposition as the main focus is on the impact of adaptive meshing as a tool to improve and accelerate ash dispersion forecast models.

In the following we first introduce the implementation of the adaptive semi-Lagrangian advection algorithm and explain how the sedimentation of particles has been implemented into this model. We then turn to the description of our case study of the climactic eruption of Mt. Pinatubo, 1991. Here we focus first on the main advantages of our solution and then carry out a sensitivity analysis by varying different input parameters. We finish with some discussion (including a detailed performance study) and conclusion.

2 Model description

In the model we solve the advection equation in conservation form

$$\frac{\mathrm{d}C}{\mathrm{d}t} = R, \text{ with } \frac{\mathrm{d}C}{\mathrm{d}t} = \frac{\partial C}{\partial t} + \nabla \cdot (\boldsymbol{u} C) = R, \tag{1}$$

where $C(x,y,z,t) = C(\mathbf{x},t)$ is a scalar concentration, $\boldsymbol{u} = (u_x, u_y, u_z)^\top$ is a given wind field, and R is ~~the so called~~ a right hand side ~~which can include additional forces as well as~~ implementing sources and sinks~~for the scalar tracer concentration $C(x,y,z)$. In our case~~. As usual, we will denote with $(x,y,z) = \mathbf{x}$ and t the spatial and time coordinate, respectively. Using the integral form of this conservation law

$$\frac{d}{dt} \int_{V(t)} C(\mathbf{x},t)\, d\mathbf{x} = R, \tag{2}$$

where $V(t)$ is a (time-dependent) reference volume, we can derive a semi-Lagrangian discretization

$$\int_{V(t)} C(\mathbf{x},t)\, d\mathbf{x} = \int_{V(t-\Delta t)} C(\mathbf{x},t-\Delta t)\, d\mathbf{x} + \Delta t R. \tag{3}$$

Following the description in (Behrens, 2006) the integral expressions can be discretized by a mid-point rule, multiplying the point value of concentration $C(\mathbf{x},t)$ with the area of the dual cell $\bar{V}(\mathbf{x},t)$ corresponding to grid point $\mathbf{x}$. We obtain

$$\begin{aligned} |\bar{V}(\mathbf{x},t)| \cdot C(\mathbf{x},t) &\approx |\bar{V}(\mathbf{x}-\alpha, t-\Delta t)| \cdot C(\mathbf{x}-\alpha, t-\Delta t) + \Delta t R, \\ \Rightarrow C(\mathbf{x},t) &\approx \frac{|\bar{V}(\mathbf{x}-\alpha,t-\Delta t)|}{|\bar{V}(\mathbf{x},t)|} C(\mathbf{x}-\alpha,t-\Delta t) + \Delta t R, \end{aligned}$$

where α is the semi-Lagrangian upstream displacement from a given grid point, and R ~~includes the volcanic source (for implementation in our case see below)~~is evaluated at the upstream position. Note that the cell area corresponding to the concentration point changes in time and – depending on the velocity field – may be distorted, such that mass is conserved even in non-divergent flow fields. This scheme deviates from a point-wise semi-Lagrangian method as described in (Staniforth and Cote, 1990) by the correction factor $\frac{|\bar{V}(\mathbf{x}-\alpha,t-\Delta t)|}{|\bar{V}(\mathbf{x},t)|}$. It is unconditionally stable as long as $\bar{V}(\mathbf{x},t)$ does not degenerate.

In order to compute the areas $|\bar{V}(\mathbf{x}-\alpha,t-\Delta t)|$ and $|\bar{V}(\mathbf{x},t)|$ on a non-uniform tetrahedral mesh simple computational geometry methods are used. The upstream value $C(\mathbf{x}-\alpha,t-\Delta t)$ is interpolated by a linear interpolation within the upstream

tetrahedron. While linear interpolation is theoretically very dissipative, it is positivity preserving and monotonous and in combination with the local mesh refinement described below only small numerical smoothing is observed.

The advection of the cloud is driven by a pre-calculated wind field $\boldsymbol{u}(x, y, z)$ from the regional scale atmospheric chemistry and climate model REMOTE (**Re**gional **Mo**del with **T**racer **E**xtension), for details see ~~(Langmann, 2000)~~Langmann (2000). Initial meteorological data are taken from the ECMWF and boundary conditions are updated every 6 h. The horizontal resolution of the wind field is 0.5° × 0.5° (approximately 55 km × 55 km). In the vertical direction a pressure-sigma coordinate subdivides the model atmosphere into 31 layers of increasing thickness between the Earth surface and the 10 hPa pressure level. Here we utilized all vertical layers and interpolated the wind in $x-$, $y-$ and $z-$direction to the grid resolution.

~~We solve the time dependent part of this equation by a~~ This interpolation is linear in space and time to maintain monotonicity and preserve shape of the vector field.

The semi-Lagrangian ~~method (see (Staniforth and Cote, 1990)). A finite element like method was used to solve for the spatial dependence of C. The solution is carried out on~~ method described above employs an adaptive mesh following (Behrens, 1996): in regions, where a high spatial resolution is required, the mesh is refined, whereas the mesh size in other parts of the model domain is kept relatively coarse. Thereby, memory requirements can ~~possibly~~ potentially be decreased by orders of magnitude without losing accuracy~~(Behrens, 1996)~~. In our case the refinement criterion is based on the concentration gradient $\boldsymbol{\nabla} C|_{\tau_i}$ in a mesh element $\tau_i \in T$, where the triangulation T ~~represents the complete triangulation~~denotes the complete set of tetrahedra representing the computational domain. A mesh element is refined if ~~$\boldsymbol{\nabla} C|_{\tau_i} > \theta_{\mathrm{ref}} \cdot \boldsymbol{\nabla}_{\max}$, with $\boldsymbol{\nabla}_{\max} = \max_{\tau_i \in T}\{\boldsymbol{\nabla} C|_{\tau_i}\}$~~

$$\boldsymbol{\nabla} C|_{\tau_i} > \theta_{\mathrm{ref}} \cdot \boldsymbol{\nabla}_{\max}, \tag{4}$$

with

$$\boldsymbol{\nabla}_{\max} = \max_{\tau_i \in T}\{\boldsymbol{\nabla} C|_{\tau_i}\} \tag{5}$$

being the maximum of all local concentration gradients. Accordingly, a mesh element is coarsened if ~~$\boldsymbol{\nabla} C|_{\tau_i} < \theta_{\mathrm{crs}} \cdot \boldsymbol{\nabla}_{\max}$.~~

$$\boldsymbol{\nabla} C|_{\tau_i} < \theta_{\mathrm{crs}} \cdot \boldsymbol{\nabla}_{\max}. \tag{6}$$

The parameters θ_{ref} and θ_{crs} (with $0 < \theta_{\mathrm{ref}} \leq 1$ and $\theta_{\mathrm{crs}} < \theta_{\mathrm{ref}}$) define the relative tolerances for refinement and coarsening respectively.

The *a posteriori* adaptation strategy computes local gradients in each element after each time step. This computation is cheap and requires just a few operations per element. Those elements fulfilling (4) or (6) are marked for refinement or coarsening, respectively. The mesh is only refined or coarsened, if a certain fraction $w_{\mathrm{ref/crs}}$ of grid cells is marked, in order to balance accuracy requirements with computational cost. The cell refinement/coarsening follows a bisection strategy, described in Bänsch (1991).

In our scenario computations we used the following parameters for controlling the mesh:

$$\theta_{\mathrm{ref}} = 0.02, \quad \theta_{\mathrm{crs}} = 0.005, \quad w_{\mathrm{ref/crs}} = 0.001.$$

This means that a cell is flagged for refinement, if its gradient is larger than 2% of the maximum local gradient. And the mesh is changed, if 0.1% of the cells are marked.

2.1 Particle Sedimentation

The sedimentation of tephra from an advecting ash cloud is mainly dependent on the grain size, the density of the particles and the properties (viscosity and density) of the surrounding air. In order to account for sedimentation, the terminal settling velocity v_t (balance between drag force and gravitational force) is calculated for atmospheric conditions at every mesh point and every time step. The terminal settling velocity is given by

$$v_t = \sqrt{\frac{4}{3}\frac{(\rho_p - \rho)}{\rho C_d} D_p g}, \tag{7}$$

with ρ_p the density of an ash particle with a diameter D_p, ρ the density of the surrounding fluid (calculated here from REMOTE simulation results), g the gravitational acceleration and C_d the drag coefficient. Settling of particles is then accounted for in the advection equation (Eq. 1)

$$\frac{\partial C}{\partial t} + u_x \frac{\partial C}{\partial x} + u_y \frac{\partial C}{\partial y} + (u_z - v_t)\frac{\partial C}{\partial z} = R,$$

by modifying the vertical advection term:

$$\frac{\partial C}{\partial t} + \nabla \cdot \left[(u_x, u_y, u_z - v_t)^\top C\right] = R. \tag{8}$$

The terminal settling velocity is dependent on the drag coefficient C_d which is a function of the Reynolds number Re which in turn depends on the settling velocity. Empirical formulations of the drag coefficient for different regimes of the Reynolds number have been suggested by several authors (Seinfeld and Pandis, 2006; Dellino et al., 2005; Bonadonna et al., 1998; Herzog et al., 1998; Ganser, 1993; Arastoopour et al., 1982; Wilson and Huang, 1979). Here we use the model introduced by Ganser (1993), which gave the best results for our conditions (look at the online supplement for more details).

For calculating Re the dynamic viscosity of the air in dependence on the air temperature is required (Pruppacher and Klett, 1997):

$$\mu = \begin{cases} (1.718 + 0.0049 \cdot T_C) \times 10^{-5} & T_C \geq 0°\mathrm{C} \\ (1.718 + 0.0049 \cdot T_C - 1.2 \times 10^{-5} \cdot T_C^2 \times 10^{-5} & T_C < 0°\mathrm{C}, \end{cases} \tag{9}$$

with T_C the temperature in °C.

Particles require a certain time (a so called *relaxation time*) to reach their terminal settling velocity (Seinfeld and Pandis, 2006):

$$t_r = \frac{M_p C_s}{3\pi\mu D_p}. \tag{10}$$

Here, M_p is the mass of the ash particle and C_s is a slip correction factor defined by Seinfeld and Pandis (2006).

Using reasonable values for the parameters in (10), it is obvious that the maximum time required by particles to reach their terminal settling velocity is relatively short. Even for particles with a diameter of 1 mm ($\phi = 0$) the maximum relaxation time is only about 9 s. Compared to the default simulation time step of 10 min used here and a simulation period of about five days, the relaxation time is negligible. Therefore, we assume that the ash particles are falling directly with their terminal settling velocity.

With the assumption that in dilute clouds ash particles of different sizes do not affect each other but each particle settles individually (i.e. we neglect particle aggregation as well as particle particle interaction) we apply the model for individual particle diameters and then combine the results of different runs to predict the sedimentation of the complete grain size distribution. As we model the fallout from the umbrella cloud, we furthermore assume that the ash particles already reached their maximum injection height at the start of the model. Complex eruption column dynamics are neglected and we suppose no interaction with and no re-entrainment into the eruption column. In addition, the settling of ash particles is strongly affected by rain fall and particle aggregation (see e.g. Brown et al. (2012)). Since this work is a first case study of the modeling of sedimentation of ash particles on an adaptive mesh the impact of rain on the sedimentation and aggregation of ash particles is neglected. Finally, we treat the ash particles as passive tracers and do not monitor the thickness of the ash deposited on the ground.

3 Modeling the Climactic Eruption of Mt. Pinatubo

3.1 Summary of the 1991 Mt. Pinatubo

The 1991 Mt. Pinatubo eruption on the island Luzon in the Philippines (see Fig. 1) was one of the largest explosive eruptions in the 20th Century. The amount of erupted SO_2 induced a global cooling of at least 0.5°C in the two years following the eruption (Self et al., 1996). Pyroclastic flows, lahars (thick volcanic mudflows) and ash fall made more than 50,000 people homeless, affected the lives of more than a million people and caused 200 to 300 deaths (Punongbayan et al., 1996; Bautista, 1996).

Following a quiet period of about 500 years (Newhall et al., 1996) activity at Mt. Pinatubo started in July 1990 with a magnitude 7.8 earthquake along the Philippine fault, about 100 km north-east of the summit (Punongbayan et al., 1991). Many smaller earthquakes were recorded in the following months and in April 1991 ~~,~~the first eruptions with column heights between 1 and 8 km took place. The explosive phase began on June 12, 1991 and lasted till June 16 with subplinian to plinian eruptions and column heights between 19 and 40 km. The most violent eruptions occurred between 13:40 (PDT) and 22:40 on June 15 with more or less continuous high-output activity. The intensity of this eruption period began to decrease after about three hours at 16:40 on June 15 (Wolfe and Hoblitt, 1996). In the nine hour lasting climactic eruption phase, 80 percent of the total erupted volume was ejected and the highest eruption columns were reached (Holasek et al., 1996).

During the first phase of the climactic eruption, the ash expanded radially and formed a huge umbrella cloud. Koyaguchi and Tokuno (1993) analyzed the hourly multi-spectral images of the Global Mapping Satellite (GMS) on June 15, 1991 and showed that following the onset of the climactic eruption at 13:41, the erupted material expanded radially for about five to six hours in a giant umbrella cloud. At 14:40 Koyaguchi and Tokuno (1993) identified an ash cloud of 280 km diameter in the

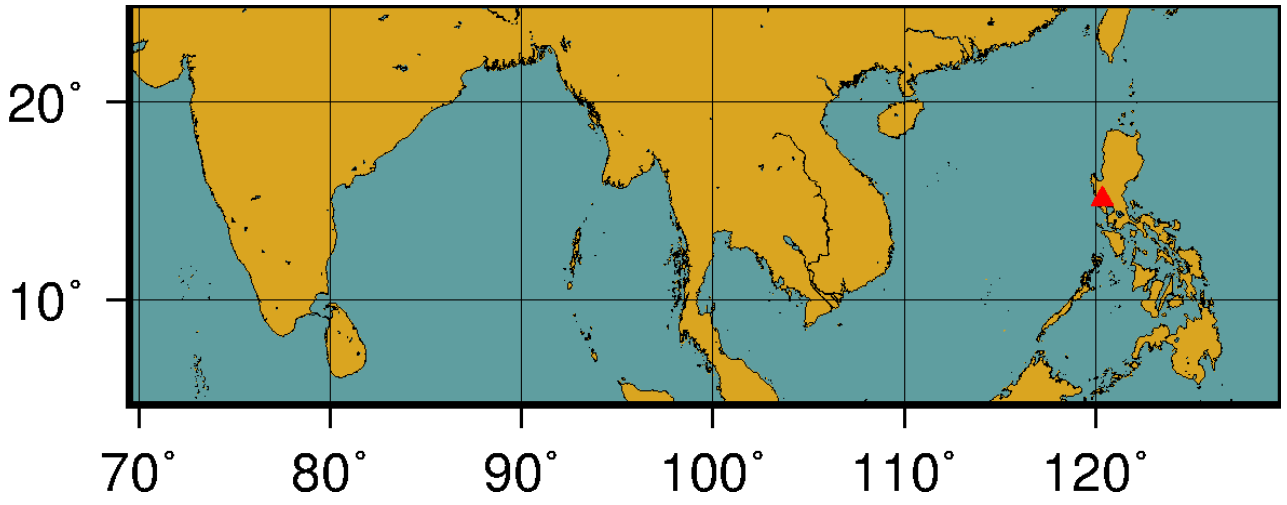

Figure 1. Location of Mt. Pinatubo marked by the triangle in the simulation domain (69.5°E/4.5°N to 130°E/25.5°N).

satellite images and at 15:40 the umbrella cloud covered an area with a diameter of 400 km. Similar studies using infrared (Lynch and Stephens, 1996) and GMS-4 visible band data were used to determine the radial expansion and advection of the ash cloud in west-southwest direction. The southwestward advection of the umbrella cloud mainly reflects the wind direction in the stratosphere (Koyaguchi and Tokuno, 1993).

Light to moderate tephra was displaced southward and moderate to heavy tephra northeastward by Typhoon Yunya which passed in a distance of about 75 km northeast of the erupting volcano at around 14:00 on June 15, 1991 (Oswalt et al., 1996). This atypical wind in the lower and middle troposphere caused by the passing typhoon lead to the wide distribution of tephra in nearly all directions around the volcano (Wolfe and Hoblitt, 1996). The heaviest tephra falls occurred during the climactic eruption on June 15, producing tephra fall deposits with up to 33 cm thickness (Paladio-Melosantos et al., 1996). An area of around 7500 km^2 on Luzon was covered by more than 1 cm thick tephra deposits and the entire island obtained at least a trace of ash (Paladio-Melosantos et al., 1996). Paladio-Melosantos et al. (1996) examined the grain sizes of the Pinatubo 1991 tephra-fall deposits on the Luzon Island relatively close to the vent ($\leq$ 30 km distance), while Wiesner et al. (1995) recorded the fallout of tephra following the climactic eruption by two sediment traps moored at 14.60°N and 115.10°at a water depth of 1190 m and 3730 m in the South China Sea.

3.2 Simulation set-up

3.2.1 Volcanic Ash Emissions

In order to properly model the source term R in (8), mass eruption rates need to be defined as model inputs. Our estimate of the mass eruption rates is based on observations by Holasek et al. (1996) in visible and infrared satellite images. For some satellite data Holasek et al. (1996) could not determine the altitude of the eruption plume and we completed values with data

Eruption phase start	Eruption phase end	Mass eruption rate [kg/~~m^3~~s]
June 13, 1991, 08:25	June 13, 1991, 08:55	5.775×10^7
June 14, 1991, 13:09	June 15, 1991, 13:41	2.1×10^7
June 15, 1991, 08:10	June 15, 1991, 10:27	9.75×10^6
June 15, 1991, 10:27	June 15, 1991, 13:41	2.25×10^7
June 15, 1991, 13:41	June 15, 1991, 22:41	2.1×10^8
June 15, 1991, 22:41	June 16, 1991, 10:41	1.5×10^7

Table 1. Eruption phases implemented in the right-hand side. For time periods not listed in this Table, the right-hand side was set to zero. The values given in italics are those for the climactic phase of the eruption. For converting m^3/s to kg/s we used an average density of 1500 kg/m^3.

from Self et al. (1996). A complete list of eruption height used to estimate mass eruption rates is given in Tab. A1. After June 16 10:41, secondary explosions were induced by the interaction of the hot ignimbrite with water, but these secondary eruption plumes were of less intensity and are not considered in this study. Holasek et al. (1996) calculated an average eruption rate of 1.4×10^5 m^3/s for the nine hour lasting climactic phase from June 15 13:41 to 22:41. Accordingly, we estimated mass eruption rates for the other eruption phases from the data of Holasek et al. (1996) and Self et al. (1996). The mass eruption rates used in this study are listed in Tab. 1.

Ash is not released evenly along the eruption column into the atmosphere but mostly close to the neutral buoyancy level. Fero et al. (2009) simulated the Pinatubo eruption with different tephra dispersal models and determined that most of the ash was advected in an umbrella cloud at the level of the tropopause at around 17 km – significantly below the maximum column heights of 40 km and below the main transport level of SO_2 at around 25 km. We follow their approach and ~~inserted ash~~ release ash over the time intervals indicated in Tab. 1 in a 4 km long cylinder with a radius between 2 and 5 degrees and a medium height of 17 km centered above Pinatubo volcano (see also Tab. 2). The size of the cylinder is varied during the sensitivity study as well as its center location in the atmosphere. ~~By dividing the mass eruption rate~~ The mass eruption rates (listed in Table 1) were divided by the cylindrical ash injection volume ~~,~~ and multiplied by the simulation time step. Thereby the particle concentration C at each mesh point ~~can be calculated for~~ and each time step during the release of ash was obtained.

Ash is settling out of the eruption cloud dependent on its grain size. Summarizing the results of Paladio-Melosantos et al. (1996) and Wiesner et al. (1995) in an area of about 600 km around the volcano, ash fallout ranges from -4 to 9 ϕ (16 to 0.00195 mm). Since large particles below 1 ϕ settle too fast and would require very small time steps and very small particles above 8 ϕ sediment outside the simulation domain, we neglected these particle sizes. For a sake of simplicity, we used a Gaussian distribution around a mean grain size of 4.5 ϕ with a standard deviation of $\sigma_\phi = 2.5$ which corresponds well with the estimated bulk mean grain size of 4 ϕ of the Pinatubo tephra deposit (Fero et al., 2009). The grain size categories used for the estimation of the settling velocities are listed together with the particle diameter and the particle density in Table 3.

Parameter	Standard value	Variation range	Units
Fine mesh refinement level	17	14 – 23	–
Coarse mesh refinement level	8	–	–
Tolerance of refinement θ_{ref}	0.02	–	–
Tolerance of coarsening θ_{crs}	0.005	–	–
Time step length	600	–	seconds
Number of time steps	684	–	–
Initial cloud radius	4	2 – 5	degree
Height of initial cloud center	17	15 – 21	km
Initial cloud thickness	6	2 – 8	km
Grain size	4.5	0 – 8	ϕ

Table 2. Parameter values used in the model calculations. For $\theta_{\mathrm{ref}}, \theta_{\mathrm{crs}}$, see eqs. (4) and (6).

Grain size [ϕ]	Diameter [mm]	Density [kg/m^3]	Wt.%
2 – 1	0.25 – 0.5	1430	4.17
3 – 2	0.125 – 0.25	1720	11.34
4 – 3	0.0625 – 0.125	2010	20.66
5 – 4	0.0313 – 0.0625	2300	25.23
6 – 5	0.0156 – 0.0313	2300	20.66
7 – 6	0.0078 – 0.0156	2300	11.34
8 – 7	0.0039 – 0.0078	2300	4.17

Table 3. Particle diameters and densities utilized in the sedimentation simulations. The particle densities as a function of the grain size listed here are extracted from Macedonio et al. (1988).

3.2.2 Mesh generation and refinement settings

The initial mesh consists of three cubes, each extending from 4.5°N to 24.5°N and from 0 to 23km height and from 69.5°E to 89.5°E (cube 1), 89.5°E to 109.5°E (cube 2) and 109.5°E to 129.5°E (cube 3). Each cube contains 6 ~~tetrahedrons~~tetrahedra, so initially there are 18 ~~tetrahedrons~~ tetrahedra in the domain. Due to the minimum refinement level of 8 (*Coarse Mesh Level* in Tab. 2) each of these ~~tetrahedrons~~ tetrahedra is refined 7 times resulting in a total of 2304 ~~tetrahedrons in the complete modeling domain~~ tetrahedra in the initial model domain before local refinement. The *Coarse Mesh Level* gives the level of global and uniform refinement at the initialization of the grid and the maximum level to which an element is coarsened, whereas the *Fine Mesh Level* defines the maximum level to which an element can be refined. After the initial refinement of the mesh (corresponding to a mesh level of 8), the minimum length of the edges of the ~~tetrahedrons~~ tetrahedra in horizontal direction is 4.5 degree. With the maximum refinement level of 17, minimum edge length of 0.6 degree in horizontal and 0.7 km in vertical direction are achieved (compare Tab. 4).

Mesh refinement	min. horizontal edge length	min. vertical edge length
Refinement level 8	4.5 degree	5.75 km
Refinement level 17	0.6 degree	0.7 km

Table 4. Minimum edge length of the ~~tetrahedrons~~ tetrahedra in horizontal and vertical direction.

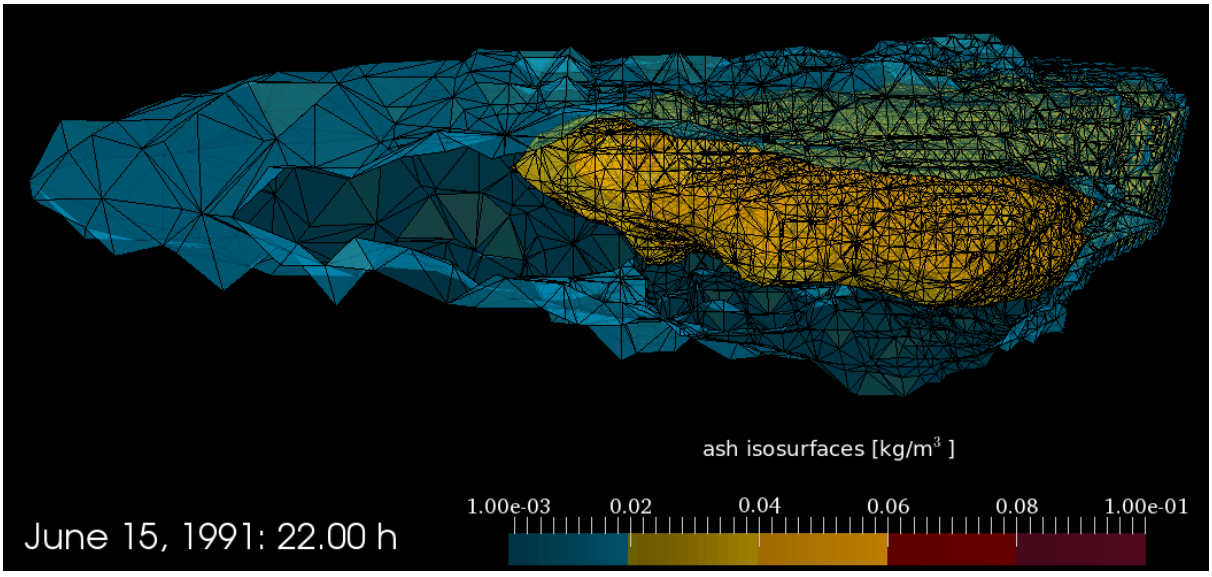

Figure 2. Triangulated mesh on the surface of the ash cloud. The ash cloud is represented on June 15 at ~~23~~22:~~30~~ 0 in a side view (from south). The concentration on the ~~surface~~ isosurfaces of the ash cloud is displayed in kg/m^3. The minimum displayed ash concentration is 0.001 kg/m^3.

In Figure 2, the structure of the three dimensional adaptive tetrahedral mesh of the ash cloud on June 15 ~~23:30~~ 22:00 PDT is displayed. The cloud is seen form the side. The mesh is composed of ~~tetrahedrons~~ tetrahedra with variable size. Please note that particle settling is not considered in this simulation. On the right side — where the mesh resolution is higher — the ash emissions are inserted into the model (see above), leading to a larger gradient in the ash concentration which in turn starts the mesh refinement dependent on the refinement and coarsening tolerances (see Tab. 2 and section 2). An animation of the advection of the three dimensional cloud can be found in the supplementary material.

The impact of the maximum level of refinement (*Fine Mesh Level*) is demonstrated in Figure 3 where a horizontal cross section at the height of the mean transport level (17 km) is shown. Between the ash clouds simulated with a *Fine Mesh Level* of 14 (Fig. 3a) and a *Fine Mesh Level* of 17 (3b), significant differences in shape and ash concentration of the clouds can be observed. When comparing the ash concentration for different mesh resolutions, it is import to consider that the total amount of ash inserted initially is slightly different for the different refinement levels, because the discrete volume of the cylinder in which the ash is inserted is dependent on the cell size. Using a *Fine Mesh Level* of 14 the discrete volume amounts to 97.6 % of

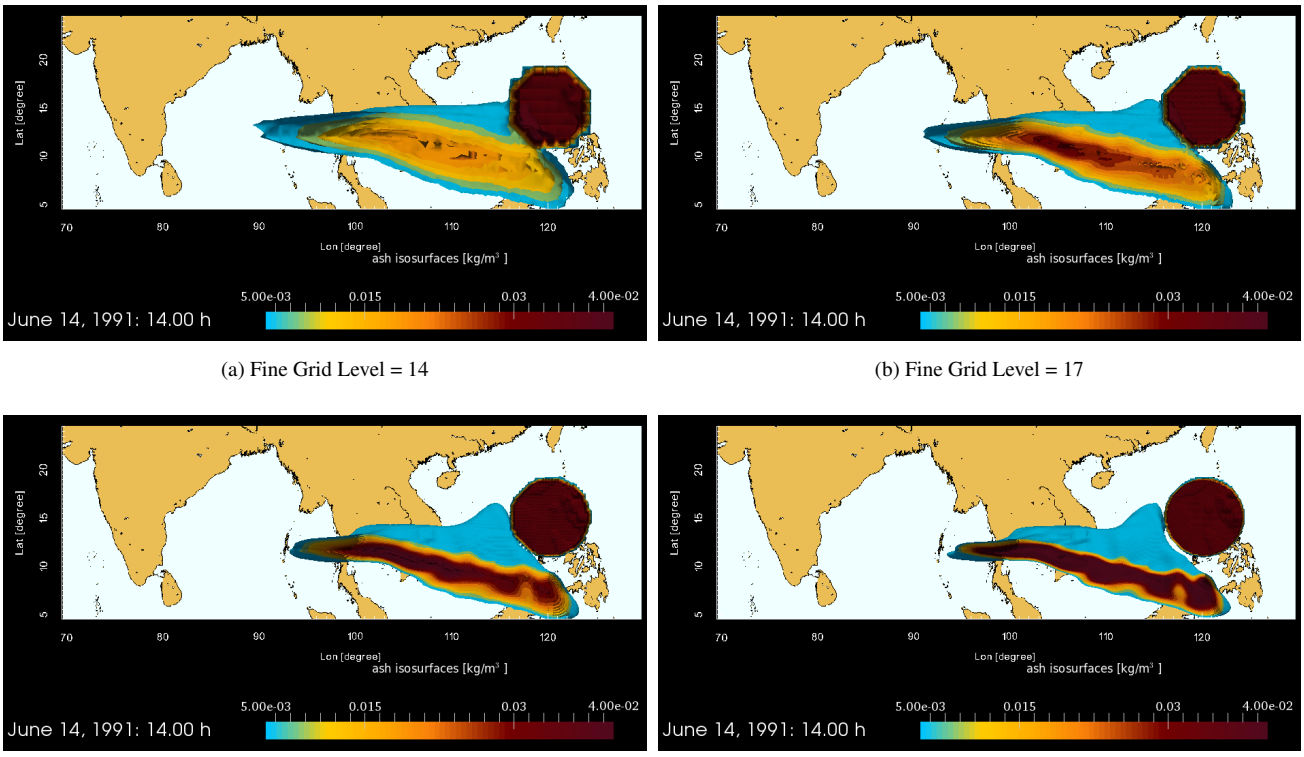

(a) Fine Grid Level = 14

(b) Fine Grid Level = 17

(c) Fine Grid Level = 20

(d) Fine Grid Level = 23

Figure 3. Horizontal cross section of the ash cloud at a height of 17 km, modeled with a *Fine Mesh Level* of 14, 17, 20 and 23. Results for June 14 at 14:00 PDT are shown. The colors indicate ash concentration in kg/m^3. The minimum displayed ash concentration is 0.005 kg/m^3.

the analytical volume of the cylinder (compare section 3.2.1) while with a *Fine Mesh Level* of 17 the inserted ash mass already accounts for 99.5 % of the original ash mass.

For *Fine Mesh Level* larger than 16, we found that the results do not change significantly any more apart from small differences in the ash concentration, but the general behavior of the ash cloud is preserved. Hence, from here on we utilize a *Fine Mesh Level* of 17 as maximum refinement level allowing for fast computation of the ash spreading.

3.3 Results for the standard model setup

Figure 4 shows the evolution of the settling ash cloud for a particle size of 4.5 ϕ (0.0469 mm) (animation in the supplement). At 10:00 on June 13, the ash cloud is centered above the volcano at a mean height of around 16 km (Fig. 4a). In the following four hours, the ash cloud is settling down to a medium height of around 13 km and is slightly advected to the west (Fig. 4b). On June 14 14:00, ash particles of the eruption on June 13 have sedimented down to the ground, while the eruption cloud from the second eruption phase starting on June 14 13:09 (compare Tab. 1) is still close to its initial position (Fig. 4c). One day later on June 15 at 14:00, shortly after the onset of the climactic eruption, the *ash column* from the second eruption phase is

centered above the South China Sea. While settling, ash particles are advected to the southwest, especially between heights of 8 to 10 km (Fig. 4d). In the following hours, the ash cloud is drifting further in southwest direction (Fig. 4e and 4f). After the last eruption phase ended (on June 16 10:41), the ash cloud is sinking down and is advected to the west-southwest (Fig. 4g and 4h).

Figure 4 only shows ash concentration on the surface of the ash cloud. Figure 5 allows a look into the ash cloud where cross sections of the iso-surfaces of the ash concentration on June 14 at 14:00 and June 15 at 22:00 are displayed. When ash is inserted, the ash concentration inside the cloud is initially homogeneous (Fig. 5a). While the ash is advected and sediments, ash particles are dispersed and the ash concentration decreases. Since ash is inserted continuously between a height of 14 to 20 km, the highest ash concentrations are obtained in the upper part of the cloud (Fig. 5b). After the onset of the climactic eruption, the ash concentration inside the cloud significantly increases~~(note that different colorbars are used)~~.

The results of the advected and sedimented ash cloud on June 15 at 22:00 are displayed for model runs with different grain sizes and for a simulation without the settling of particles in Figure 6. In the simulation without the settling of particles (Fig. 6a), most of the ash is advected in the stratosphere and upper troposphere in west- and southwestward direction. The larger the ash particles are, the higher is the settling velocity and the more is the ash advected to the south due to the changing wind patterns in the atmosphere. For particles with grain sizes of 7.5 ϕ and 6.5 ϕ, advection dominates and the ash cloud is drifting more or less horizontally to the west-southwest (Fig. 6b and 6c). The effect of sedimentation becomes visible for particle sizes larger or equal to 5.5 ϕ (Fig. 6d). For simulations with particle sizes between 4.5 and 3.5 ϕ, a certain amount of the ash particles sedimented to the ground on June 15 22:00, but advection still has an impact on the motion of the cloud (Fig. 6e and 6f). For even larger particles, sedimentation dominates the advection of ash particles and the particles are settling down in a nearly vertical ash column (Fig. 6g and 6h).

Projecting the extend of the calculated ash cloud onto satellite observations made during the Pinatubo eruption (see section 3.1) is also quite instructive to determine which particle size or sizes are the best to achieve a good fit with observations. In Figure 7a, the result of a simulation without the settling of particles is shown. The winds in the lower stratosphere advect most of the ash to the west and only a very small amount of ash travels to the southwest. For particles with a grain size of 5 ϕ (0.0313 mm), the ash settles slowly to lower altitudes, where the wind is directed southwestwardly. The particles are more or less evenly distributed between west and southwest (Fig. 7b). With increasing particle size, ash is advected in a heart-shaped cloud to the west and the southwest (Fig. 7c and 7d). The simulated ash cloud with particles of a grain size of 4 ϕ (0.0625 mm) is of a much smaller extent, because the particles are settling significantly faster and the advection of the cloud by wind plays a minor role (Fig. 7d).

Comparing all simulations with different settling velocities, the best fit to the data of Lynch and Stephens (1996) is obtained by simulations with a particle size of 5 ϕ. The agreement between the simulated ash cloud and the outline of the umbrella cloud identified by Lynch and Stephens (1996) increases, when the results for particle sizes of 4, 4.5 and 5 ϕ are combined (Fig. 8). An animation of the compared results can be found in the supplementary material. On June 15 at 22:30, the simulated ash cloud matches the data of Lynch and Stephens (1996) very well (Fig. 8a). ~~However, at~~ At 4:30 on June 16, the modeled ash

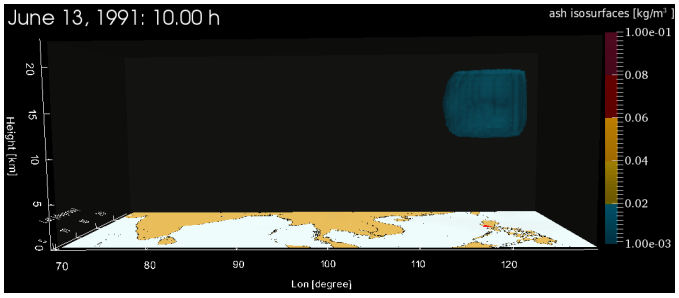

(a) June 13 10:00

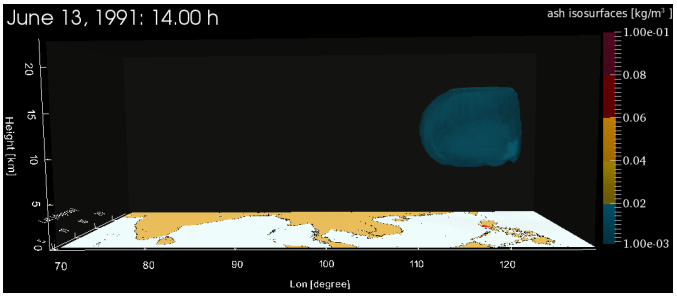

(b) June 13 14:00

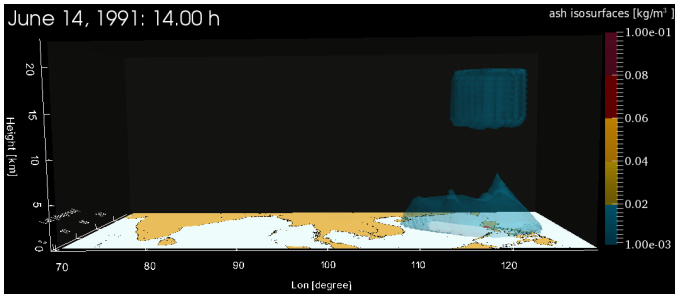

(c) June 14 14:00

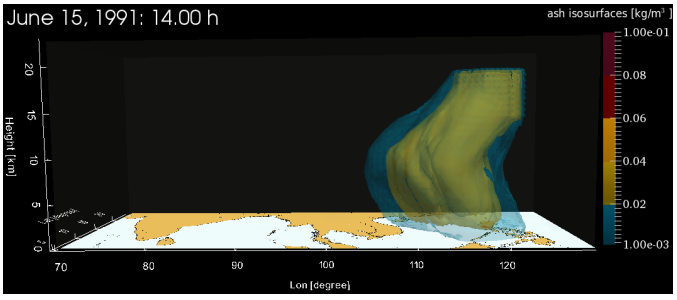

(d) June 15 14:00

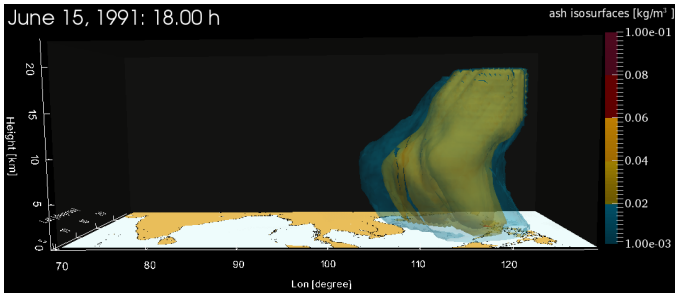

(e) June 15 18:00

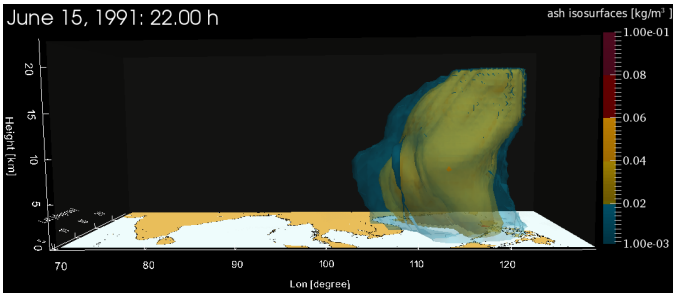

(f) June 15 22:00

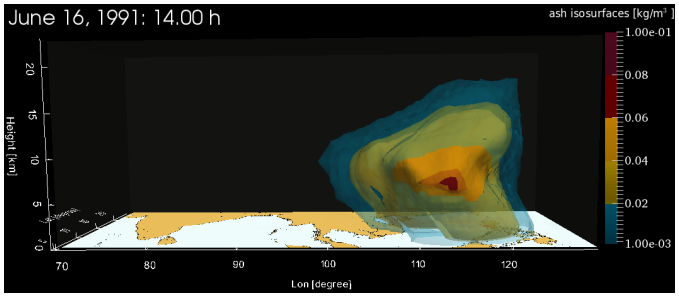

(g) June 16 14:00

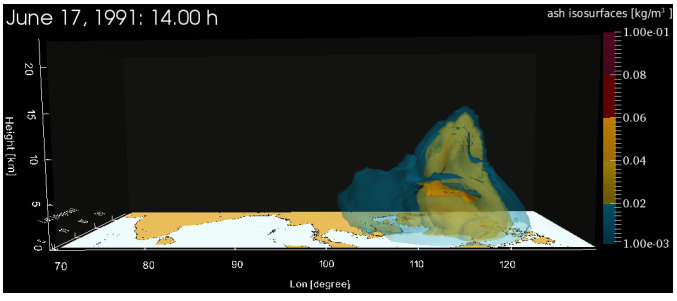

(h) June 17 14:00

Figure 4. Settling of the ash cloud over time for particles with a grain size of 4.5 ϕ. The concentration on the surface of the ash cloud is displayed in kg/m^3. Note that different colorbars are used. The minimum displayed ash concentration is 0.001 kg/m^3.

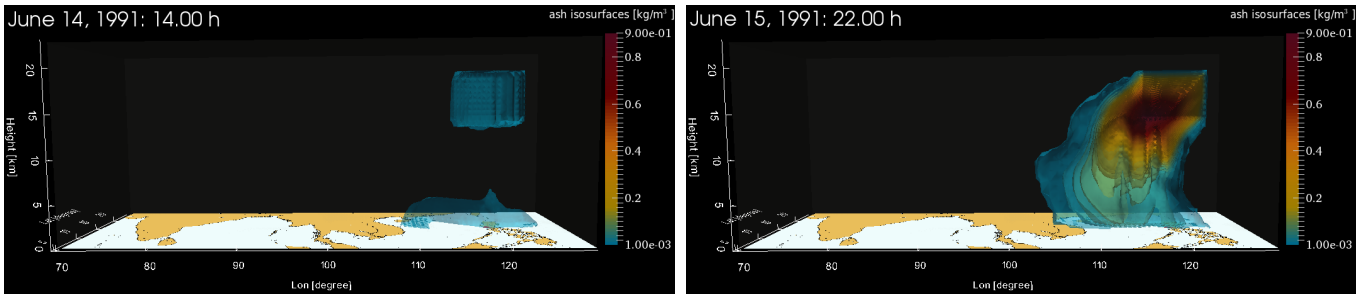

(a) June 14 14:00

(b) June 15 22:00

Figure 5. Ash concentration of the ash cloud on June 14 at 14:00 and on June 15 22:00 for particles with a grain size of 4.5 ϕ. A cross section of isosurfaces of the ash concentration is displayed in kg/m^3. ~~Note that different colorbars are used~~The minimum displayed ash concentration is 0.001 kg/m^3.

cloud and the observed contour of the ash cloud generally agree with each other, but the southern extension of the umbrella cloud could not be reproduced (Fig. 8b).

4 Discussion

In this study we adapted an existing adaptive semi-Lagrangian advection model to model the dispersion of volcanic ash emissions including the sedimentation of particles from the ash cloud. We matched our results with published satellite data of the umbrella cloud during the climactic phase of the Pinatubo eruption and found the simulation of the advection and the sedimentation to match observations quite well. The best fit between modeled and observed data were obtained by combining results from simulations with multiple particle sizes (Fig. 8b). In the following we will first test the sensitivity of our results to some of the main input parameters before we turn to a discussion of the performance advantage of our model compared to fixed grid models.

4.1 Sensitivity study

Table 2 lists various input parameters used in the model calculations. Since the initial radial expansion of the Pinatubo cloud is not included in our model, the initial radius of the ash cloud was chosen to be relatively large. In the models of Fero et al. (2009), an initial radius of around 400 km was found to be necessary to account for the radial expansion. We varied the radius between two and five degrees (approximately 222 to 555 km). Following Fero et al. (2009), most of the ash was advected at a height of around 17 km, but some amount of the ash was injected at much higher altitudes (Holasek et al., 1996). We therefore tested medium cloud heights between 15 and 21 km. Koyaguchi (1996) reported, that the thickness of the umbrella cloud was between 3 to 5 km, while Self et al. (1996) mentioned a cloud thickness of 10 to 15 km. We therefore varied the umbrella cloud thickness between 2 to 8 km. Varying the cloud thickness between 2 and 8 km height did not impact the ash dispersion

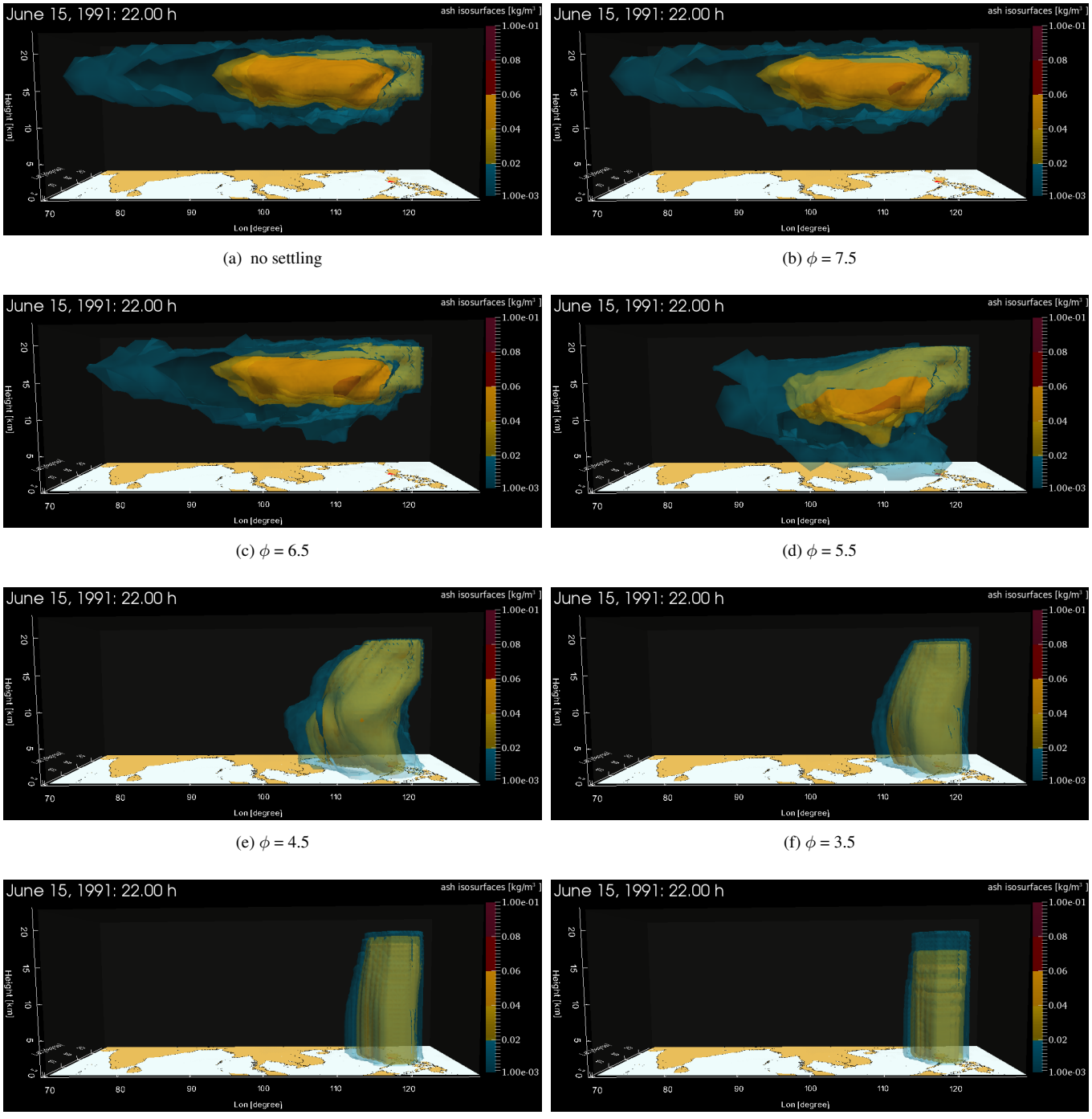

(a) no settling

(b) $\phi = 7.5$

(c) $\phi = 6.5$

(d) $\phi = 5.5$

(e) $\phi = 4.5$

(f) $\phi = 3.5$

(g) $\phi = 2.5$

(h) $\phi = 1.5$

Figure 6. Modelled ash cloud for the grain size categories listed in Table 3 and for a simulation neglecting the settling of particles. The concentration on the surface of the ash cloud is displayed in kg/m^3. ~~Note that different colorbars are used~~The minimum displayed ash concentration is 0.001 kg/m^3.

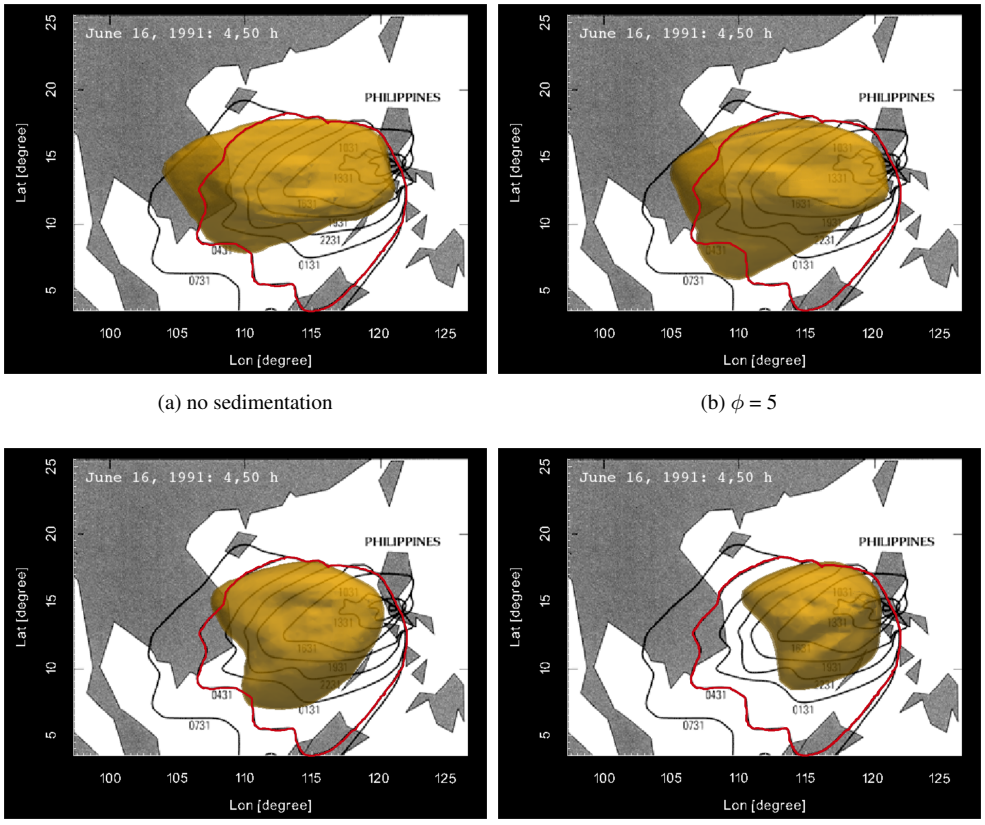

(a) no sedimentation

(b) $\phi = 5$

(c) $\phi = 4.5$

(d) $\phi = 4$

Figure 7. Advected ash cloud on June 16 4:30 for particle sizes of 4, 4.5 and 5 ϕ and for a simulation without the settling of particles. In the background, the outer edge of the observed ash cloud is displayed in three hour intervals ~~(Observed contours from: Lynch and Stephens (1996)~~(observed contours from: Lynch and Stephens, 1996)). The outer edge of the simulated ash cloud was defined as the isosurface with an ash concentration of 0.05 kg/m^3, producing the closest fit to the observed data. Note that the observational contour that corresponds to our model time (June 16 4:30) is marked in red.

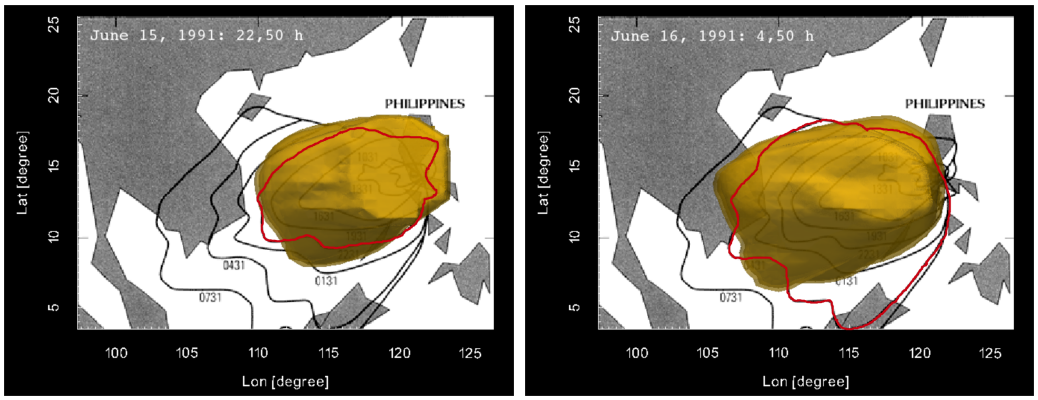

(a) June 15 22:30

(b) June 16 4:30

Figure 8. Combined results for particle sizes of 4, 4.5 and 5 ϕ and the outline of the umbrella cloud identified by Lynch and Stephens (1996).

significantly so this is not discussed in further detail below. In the following sensitivity analysis we use a medium grain size of 4.5 ϕ (0.0469 mm) in order to not obscure the results by the differences in settling velocities.

The ~~influence~~ impact of the initial cloud radius is shown in Figure 9. The ash cloud was simulated with an initial cloud thickness of 6 km, a medium height of 17 km, a grain size of 4.5 ϕ and an initial radius of 2, 3, 4 and 5°. The area covered by the cloud decreases with a decreasing radius and the shape of the modeled ash cloud becomes more circular for larger radii (compare Fig. 9a and 9d). At 22:30 on June 15, the best fit to the outline of the observed ash cloud (identified by Lynch and Stephens (1996)) is obtained with an initial cloud radius of 4°.

Figure 10 shows the effect of variation in the initial mean cloud height on the extent of the simulated ash cloud. The higher the ash is inserted, the more the cloud is advected to the west by stratospheric winds (Fig. 10d). At lower altitudes, wind mainly carries the ash in southwest direction and the ash cloud covers a heart-shaped area (Fig. 10a). The modeled ash clouds with an initial height of 17 and 19 km (Fig. 10b and 10c) better matches the contour of the ash cloud identified by Lynch and Stephens (1996), but the expansion of the umbrella cloud to the south is not reproduced.

Since non of our ~~model~~ simulations, even the best fit one shown in Figure 9, do match the observations completely — in particular in the south — we attribute the remaining differences between the modeled and the observed ash dispersion to the following facts:

1. The initial conditions of the eruption cloud are not well-known, including the vertical mass distribution in the plume.
2. The radial expansion of the umbrella cloud is accounted for by a larger initial cloud radius, which might induce deviations in cloud shape.
3. The pre-calculated wind field might not reproduce correctly the conditions during the eruption, especially the pass by of Typhoon Yunya.

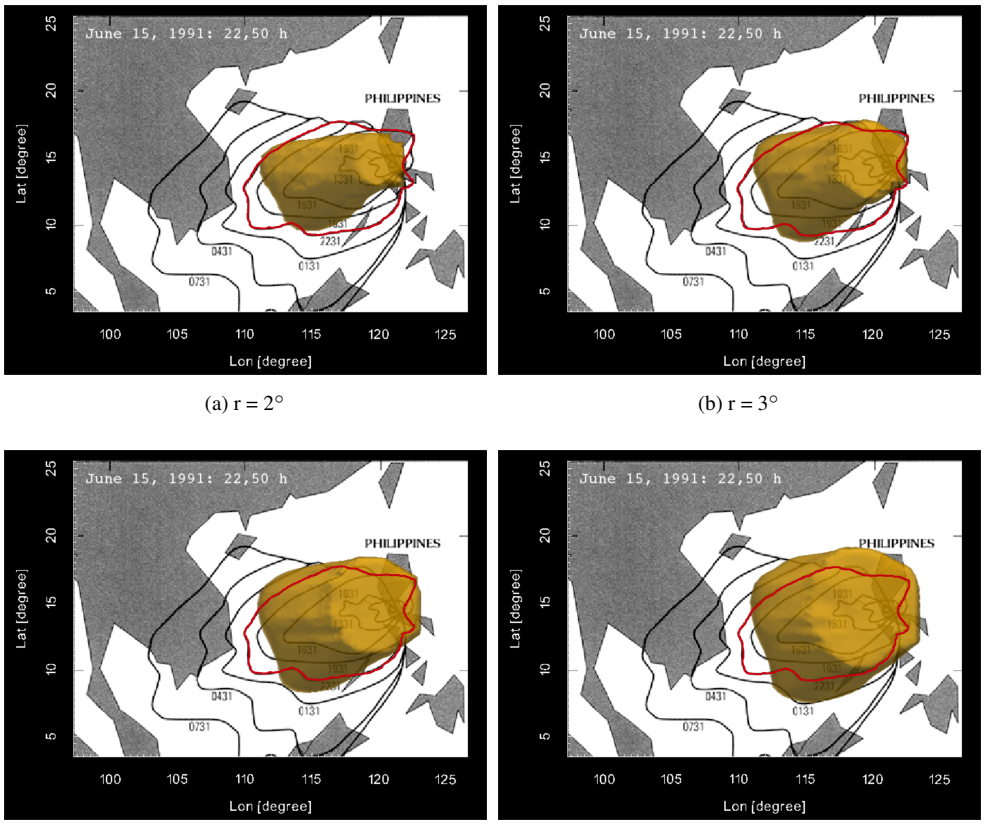

(a) r = 2° (b) r = 3°

(c) r = 4° (d) r = 5°

Figure 9. The modelled ash cloud on June 15 22:30 with an initial radius of 2, 3, 4 and 5°and the outer edge of the observed umbrella cloud in three hour intervals (observed outlines from: Lynch and Stephens (1996)). The modelled ash cloud is displayed for June 15 22:30.

4. The heavy rain caused by Typhoon Yunya is neglected in this model simulations, so that wash-out and vertical transport ~~might~~ will be underestimated.
5. Uncertainties in the outline of the umbrella cloud identified by Lynch and Stephens (1996). Satellite observations only reflect the outer contours of the ash cloud in the upper most layers. In addition, ash clouds are hard to distinguish from meteorological clouds.
6. Negligence of ash aggregation in the model calculation.

4.2 Performance due to adaptive meshing

The main advantage of this model is the use of an adaptive tetrahedral mesh leading to significantly reduced computational costs while tracking the volcanic emissions with a very high local mesh resolution. In order to determine the advantage of our adaptive meshing approach compared to fixed grid calculations we carried out a series of model runs with a fixed grid (i.e.

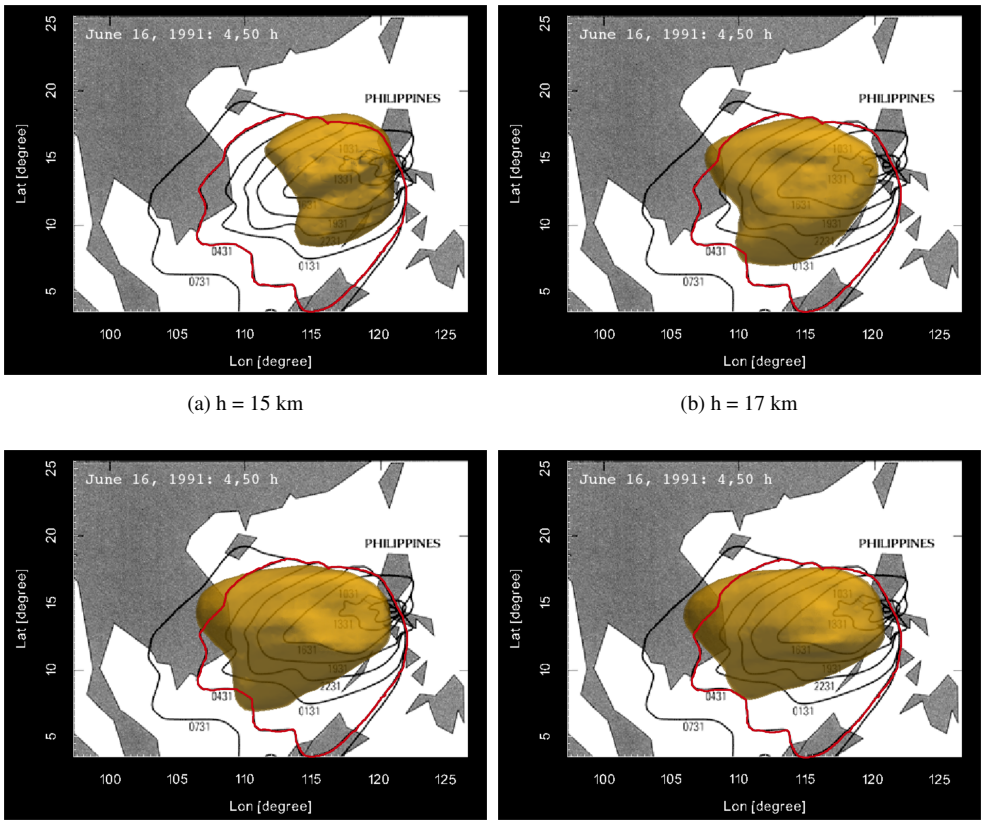

(a) h = 15 km

(b) h = 17 km

(c) h = 19 km

(d) h = 21 km

Figure 10. Advected ash cloud on June 16 4:30 inserted at a mean height of 15, 17, 19 and 21 km in combination with the extent of the observed ash cloud analyzed by Lynch and Stephens (1996).

we set the fine grid level equal to the coarse grid level to achieve a fixed grid) and compare them to our standard run with an adaptive mesh. In this case study, all simulation are carried out without the sedimentation of particles. In Figure 11, results of simulations on an uniform grid with refinement levels of 13, ~~14 and~~ 15 and 17 are compared to a result of a calculation on the adaptive mesh. ~~Obviously, the~~ The shape of the ash cloud is recovered quite well in all calculations, but small patterns in the shape and the ash concentrations are much better recovered with the finer grid structure. As mentioned above (section 3.2.2), the initial ash mass varies slightly for different mesh resolutions.

In Fig. 12 we compare the computational costs of the different model calculations. The simulation on the adaptive mesh needed only about 50 min, while the calculation on an uniform mesh with a fine grid level of 17 (i.e. the same maximum local resolution as in our adaptive mesh calculation) required already around 9 h. Those significantly reduced computational cost would allow for ensemble runs with varying meteorological boundary conditions as well as different ash injection assumptions to better constrain and forecast probable dispersion patterns and directions (see e.g. (Madankan et al., 2014)).

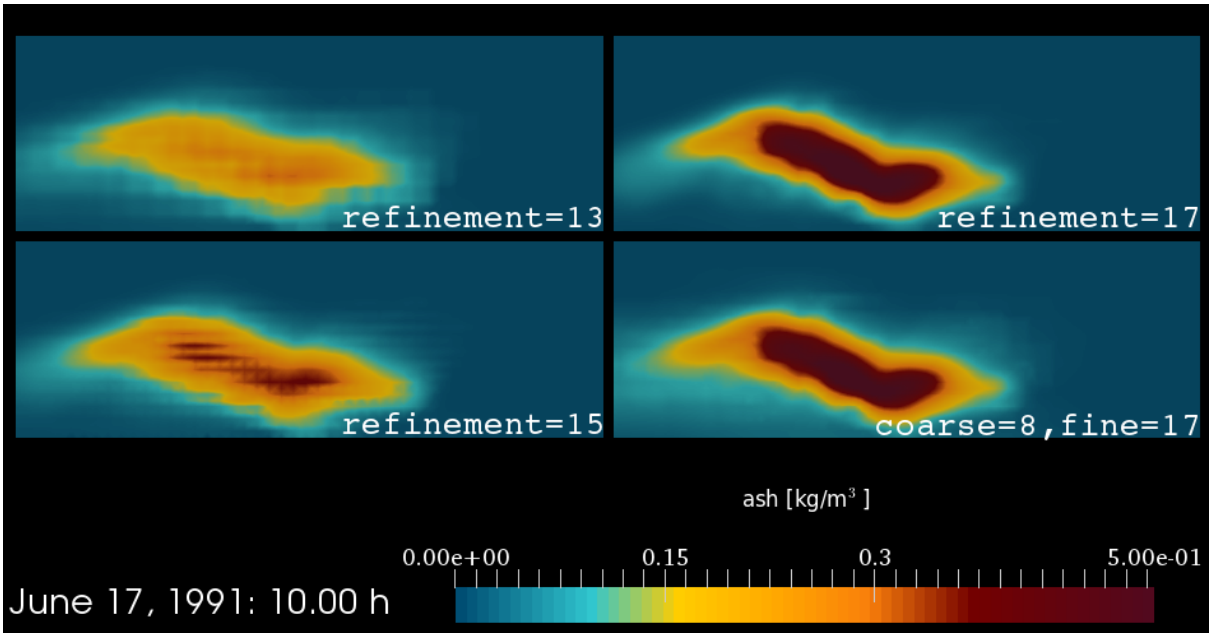

Figure 11. Comparison between simulations on an uniform mesh with a refinement level of 13 (top left), ~~14~~ 15 (lower left) and ~~15~~ 17 (top right) and a simulation on the adaptive mesh with a coarse mesh level of 8 and a fine mesh level of 17 (downright). Cross sections at a height of 18 km on June 17 at 13:20. The same figure including the mesh structure can be found in the online supplement.

5 Conclusions

In this study we have demonstrated the versatility of adaptive meshing algorithms for modeling the dispersion of volcanic emissions. Especially the high performance of this code would allow, if implemented into operational ash dispersion models, a significant improvement of dispersion predictions as model runs could be carried out significantly faster compared to codes using a fixed grid. The research community benefits from such a faster code by being able to resolve the fine filamented structure of volcanic emissions during their transport as well as test more boundary conditions, newly developed sedimentation models (e.g. (Bagheri and Bonadonna, 2016)) and complex chemical reactions which could occur between different trace gases in the atmosphere while being transported (e.g. (Hoshyaripour et al., 2015))

In our sensitivity study we have shown that the initial conditions of the ash cloud significantly influence the region impacted by the ash cloud. Even in cases where meteorological predictions, the initial height, the extent of the ash cloud as well as the mean grain size of the erupted particles are not very well constrained, our model could be used for forecasting the advection and the sedimentation of ash after a volcanic eruption through ensemble runs and thereby contribute to assessment and mitigation of risks, posed by drifting ash clouds.

A further application of the model is to predict the ash loading on the Earth's surface from tephra fallout which only needs an additional two-dimensional array to sum up the deposited ash.

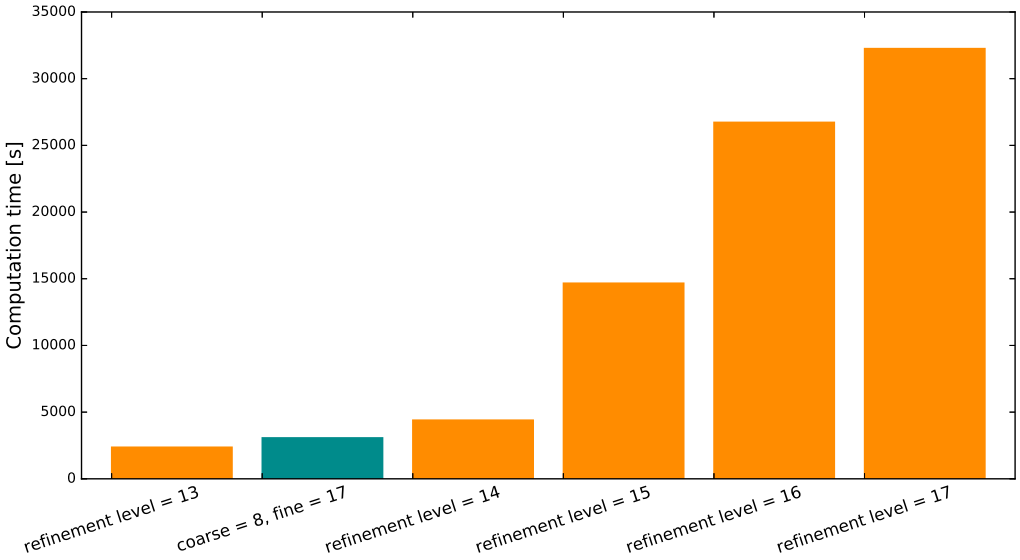

Figure 12. Comparison of the computation times of simulations on an uniform mesh with refinement levels of 13, 14, 15, 16 and 17 and on the adaptive mesh with a coarse mesh level of 8 and a fine mesh level of 17. Calculations were carried out on a lenovo thinkpad with an i3-2310M processor and 8 GB of main memory.

In order to enable the above mentioned application fields, we envision several extensions of our model. First, a more realistic tephra reaction and aggregation model could be implemented. Methodologically, this is a relatively straight forward extension of the right hand side of equation (1). Secondly, a multi-component tephra simulation could be implemented. In order to support adaptive mesh refinement for multiple grain sizes with their own sedimentation rates, a combined criterion would be necessary, which could be an additive combination of the individual component's refinement criteria. Finally, higher order interpolation for the semi-Lagrangian time stepping could further increase accuracy.

Acknoledgements

We would like to thank our reviewers, A. Folch and M. Herzog, who helped to improve the manuscript substantially. The authors acknowledge support by the Cluster of Excellence CliSAP (EXC177), Universität Hamburg, funded by the German Science Foundation (DFG).

Appendix A

Date 1991	Time [PDT]	Column Height [km]
June 13	08:41	24.0
June 14	13:09	21.0
	13:41	22.5
	14:10	15.0
	15:41	19.0
	18:53	$\geq$ 24.0
	19:41	20.0
	22:18	5.0
	23:20	21.0
	23:30	$\geq$ 21.0
	23:41	18.0
June 15	01:14	23 – 25
	01:41	21.5
	03:41	20.5
	05:55	12 – 20
	06:34	20.5
	08:10	12 – 20
	08:41	17.5
	10:27	$>$ 20
	10:41	21.5
	12:13	8.0
	12.34	24.5
June 15	13:41	37.5
	14:41	40.0
	15:41	38.0
	16:41	32.0
	17:41	34.5
	18:34	35.0
	19:41	29.0
	20:41	28.0
	21:41	27.0
	22:31	26 – 28
	22:41	26.5
	23:41	22.5
June 16	01:41	20.0
	02:41	19.0
	03:41	17.5
	04:41	16.0
	05:41	14.0
	06:41	14.0
	07:41	14.0
	08:41	13.0
	10:41	15.0
June 16 – 18		0.2 – 19

Table A1. Chronology of eruption column heights between June 13 06:00 and June 18 00:00. Data compiled from Holasek et al. (1996) and Self et al. (1996)

References

Arastoopour, D., Wang, C., and Weil, S.: Particle-particle interaction force in a dutile gas-solid system, Chemical Engineering Science, 37, 1379 – 1386, doi:10.1016/0009-2509(82)85010-0, 1982.

Bagheri, G. and Bonadonna, C.: On the drag of freely falling non-spherical particles, Powder Technology, 301, 526 – 544, doi:http://dx.doi.org/10.1016/j.powtec.2016.06.015, http://www.sciencedirect.com/science/article/pii/S0032591016303539, 2016.

Barsotti, S., Neri, A., and Scire, J. S.: The VOL-CALPUFF model for atmospheric ash dispersal: 1. Approach and physical formulation, Journal of Geophysical Research: Solid Earth, 113, doi:10.1029/2006JB004623, http://dx.doi.org/10.1029/2006JB004623, b03208, 2008.

Bautista, C. B.: The Mount Pinatubo Disaster and the People of Central Luzon, pp. 151–161, Quezon City : Philippine Institute of Volcanology and Seismology ; Seattle : University of Washington Press, http://pubs.usgs.gov/pinatubo/cbautist/index.html, 1996.

Behrens, J.: An Adaptive Semi-Lagrangian Advection Scheme and Its Parallelization, Monthly Weather Review, 124, 2386–2395, 1996.

Behrens, J.: Adaptive Atmospheric Modeling – Key techniques in grid generation, data structures, and numerical operations with applications, vol. 54 of *LNCSE*, Springer Verlag, Heidelberg, Berlin, doi:10.1007/3-540-33383-5, 2006.

Behrens, J., Dethloff, K., Hiller, W., and Rinke, A.: Evolution of Small-Scale Filaments in an Adaptive Advection Model for Idealized Tracer Transport, Monthly Weather Review, 128, 2976–2982, 2000.

Bonadonna, C., Ernst, G. G. J., and Sparks, R. S. J.: Thickness variations and volume estimates of tephra fall deposits: the importance of particle Reynolds number, Journal of Volcanology and Geothermal Research, 81, 173 – 187, 1998.

Bonadonna, C., Connor, C. B., Houghton, B. F., Connor, L., Byrne, M., Laing, A., and Hincks, T. K.: Probabilistic modeling of tephra dispersal: Hazard assessment of a multiphase rhyolitic eruption at Tarawera, New Zealand, Journal of Geophysical Research: Solid Earth, 110, n/a–n/a, doi:10.1029/2003JB002896, http://dx.doi.org/10.1029/2003JB002896, b03203, 2005.

Brown, R., Bonadonna, C., and Durant, A.: A review of volcanic ash aggregation., Physics and chemistry of the earth, parts A/B/C., 45-46, 65–78, http://dro.dur.ac.uk/14466/, 2012.

Bänsch, E.: Local mesh refinement in 2 and 3 dimensions, Impact Comput. Sci. Eng., 3, 181 – 191, 1991.

Clarkson, R. J., Majewicz, E. J., and Mack, P.: A re-evaluation of the 2010 quantitative understanding of the effects volcanic ash has on gas turbine engines, Proceedings of the Institution of Mechanical Engineers, Part G: Journal of Aerospace Engineering, 0 (0), 1 – 18, 2016.

Dellino, P., Mele, D., Bonasia, R., Braia, G., Volpe, L. L., and Sulpizio, R.: The analysis of the influence of pumice shape on its terminal velocity, Geophysical Research Letters, 32, n/a – n/a, doi:10.1029/2005GL023954, 2005.

Fero, J., Carey, S. N., and Mirrill, J. T.: Simulating the dispersal of tephra from the 1991 Pinatubo eruption: Implications for the formation of widespread ash layers, Journal of Volcanology and Geothermal Research, 186, 120 – 131, 2009.

Folch, A.: A review of tephra transport and dispersal models: Evolution, current status, and future perspectives, Journal of Volcanology and Geothermal Research, 235-236, 96 – 115, doi:http://dx.doi.org/10.1016/j.jvolgeores.2012.05.020, http://www.sciencedirect.com/science/article/pii/S0377027312001588, 2012.

Folch, A., Costa, A., and Macedonio, G.: FALL3D: A computational model for transport and deposition of volcanic ash, Computers & Geosciences, 35, 1334 – 1342, 2009.

FOUNDATION, F. S., ed.: Volcanic Hazards and Aviation Safety: Lessons of the Past Decade, 1993.

Ganser, G. H.: A rational approach to drag prediction of spherical and nonspherical particles, Powder Technology, 77, 143 – 152, 1993.

Herzog, M., Graf, H.-F., Textor, C., and Oberhuber, J. M.: The effect of phase changes of water on the development of volcanic plumes, Journal of Volcanology and Geothermal Research, 87, 55 – 74, 1998.

Holasek, R. E., Self, S., and Woods, A. W.: Satellite observations and interpretations of the 1991 Mount Pinatubo eruption plumes, Journal of Geophysical Research, 101, 27,635 – 27,655, b12, 1996.

Horwell, C. J. and Baxter, P. J.: The respiratory health hazards of volcanic ash: a review for volcanic risk mitigation, Bulletin of Volcanology, 69, 1–24, doi:10.1007/s00445-006-0052-y, http://dx.doi.org/10.1007/s00445-006-0052-y, 2006.

Hoshyaripour, G. A., Hort, M., and Langmann, B.: Ash iron mobilization through physicochemical processing in volcanic eruption plumes: a numerical modeling approach, Atmospheric Chemistry and Physics, 15, 9361–9379, doi:10.5194/acp-15-9361-2015, http://www.atmos-chem-phys.net/15/9361/2015/, 2015.

Jones, A., Thomson, D., Hort, M., and Devenish, B.: The U.K. Met Office's Next-Generation Atmospheric Dispersion Model, NAME III, in: Air Pollution Modeling and Its Application XVII, edited by Borrego, C. and Norman, A.-L., pp. 580–589, Springer US, doi:10.1007/978-0-387-68854-1_62, http://dx.doi.org/10.1007/978-0-387-68854-1_62, 2007.

Ken Salazar, M. K. M., ed.: Encounters of aircraft with volcanic ash clouds: A compilation of known incidents, 1953-2009, 545, 2010.

Koyaguchi, T.: Volume Estimation of Tephra-Fall Deposits from the June 15, 1991, Eruption of Mount Pinatubo by Theoretical and Geological Methods, pp. 583–600, Quezon City : Philippine Institute of Volcanology and Seismology ; Seattle : University of Washington Press, http://pubs.usgs.gov/pinatubo/koya/index.html, 1996.

Koyaguchi, T. and Tokuno, M.: Origin of the giant eruption cloud of Pinatubo, June 15, 1991, Journal of Volcanology and Geothermal Research, 55, 85 – 96, doi:http://dx.doi.org/10.1016/0377-0273(93)90091-5, http://www.sciencedirect.com/science/article/pii/0377027393900915, 1993.

Langmann, B.: Numerical modemodel of regional scale transport and phochemistry directly together with meteorological processes, Atmospheric Environment, 34, 3585 – 3598, 2000.

Lynch, J. S. and Stephens, G.: Mount Pinatubo: A Satellite Perspective of the June 1991 Eruptions, pp. 637–646, Quezon City : Philippine Institute of Volcanology and Seismology ; Seattle : University of Washington Press, http://pubs.usgs.gov/pinatubo/lynch/index.html, 1996.

Macedonio, G., Pareschi, M. T., and Santacroce, R.: A Numerical Simulation of the Plinian Fall Phase of 79 A.D. Eruption of Vesuvius, Journal of Geophysical Research, 93, 14,817 – 14,827, 1988.

Macedonio, G., Costa, A., and Longo, A.: A computer model for volcanic ash fallout and assessment of subsequent hazard, Computers & Geosciences, 31, 837 – 845, doi:http://dx.doi.org/10.1016/j.cageo.2005.01.013, http://www.sciencedirect.com/science/article/pii/S0098300405000269, 2005.

Madankan, R., Pouget, S., Singla, P., Bursik, M., Dehn, J., Jones, M., Patra, A., Pavolonis, M., Pitman, E., Singh, T., and Webley, P.: Computation of probabilistic hazard maps and source parameter estimation for volcanic ash transport and dispersion, Journal of Computational Physics, 271, 39 – 59, doi:http://dx.doi.org/10.1016/j.jcp.2013.11.032, http://www.sciencedirect.com/science/article/pii/S0021999113007948, frontiers in Computational Physics, 2014.

Newhall, C. G., Daag, A. S., Delfin, F. G., Hoblitt, R. P., McGeehin, J., Pallister, J. S., Regalado, M. T. M., Rubin, M., Tubianosa, B. S., Tamayo, R. A., and Umbal, J. V.: Eruptive History of Mount Pinatubo, pp. 165–195, Quezon City : Philippine Institute of Volcanology and Seismology ; Seattle : University of Washington Press, http://pubs.usgs.gov/pinatubo/newhall/index.html, 1996.

Oberhuber, J. M., Herzog, M., Graf, H.-F., and Schwanke, K.: Volcanic plume simulation on large scales, Journal of Volcanology and Geothermal Research, 87, 29 – 53, doi:http://dx.doi.org/10.1016/S0377-0273(98)00099-7, http://www.sciencedirect.com/science/article/pii/S0377027398000997, 1998.

Oswalt, J. S., Nichols, W., and O'Hara, J. F.: Meteorological Observations of the 1991 Mount Pinatubo Eruption, pp. 625–636, Quezon City : Philippine Institute of Volcanology and Seismology ; Seattle : University of Washington Press, http://pubs.usgs.gov/pinatubo/oswalt/index.html, 1996.

Paladio-Melosantos, M. L. O., Solidum, R. U., Scott, W. E., Quiambao, R. B., Umbal, J. V., Rodolfo, K. S., Tubianosa, B. S., Reyes, P. J. D., Alonso, R. A., and Ruelo, H. B.: Tephra Falls of the 1991 Eruptions of Mount Pinatubo, p. 12030, Quezon City : Philippine Institute of Volcanology and Seismology ; Seattle : University of Washington Press, http://pubs.usgs.gov/pinatubo/paladio/index.html, 1996.

Pfeiffer, T., Costa, A., and Macedonio, G.: A model for the numerical simulation of tephra fall deposits, Journal of Volcanology and Geothermal Research, 140, 273 – 294, 2005.

Pruppacher, H. R. and Klett, J. D.: Microphysics of Clouds and Precipitation, Kluwer Academic Publishers, 2nd edition edn., 1997.

Punongbayan, R. S., Rimando, R. E., Daligdig, J. A., Besana, G. M., Daag, A. S., Nakata, T., and Tsutsumi, H.: The 16 July 1990 Luzon Earthquake Ground Rupture, pp. 1 – 32, Manila, Department of Environment and Natural Resources, 1991.

Punongbayan, R. S., Newhall, C. G., Bautista, M. L. P., Garcia, D., Harlow, D. H., Hoblitt, R. P., Sabit, J. P., and Solidum, R. U.: Eruption Hazard Assessments and Warnings, pp. 415–433, Quezon City : Philippine Institute of Volcanology and Seismology ; Seattle : University of Washington Press, http://pubs.usgs.gov/pinatubo/punong2/index.html, 1996.

Robock, A.: Volcanic eruptions and climate, Reviews of Geophysics, 38, 191–219, doi:10.1029/1998RG000054, http://dx.doi.org/10.1029/1998RG000054, 2000.

Schwaiger, H. F., Denlinger, R. P., and Mastin, L. G.: Ash3d: A finite-volume, conservative Numerical Model for ash transport and Tephra deposition, Journal of Geophysical Research, 117, n/a – n/a, doi:10.1029/2011JB008968, 2012.

Searcy, C., Dean, K., and Stringer, W.: PUFF: A high-resolution volcanic ash tracking model, Journal of Volcanology and Geothermal Research, 80, 1 – 16, doi:http://dx.doi.org/10.1016/S0377-0273(97)00037-1, http://www.sciencedirect.com/science/article/pii/S0377027397000371, 1998.

Seinfeld, J. H. and Pandis, S. N.: Atmospheric Chemistry and Physics, John Wiley & Sons, 2nd edition edn., 2006.

Self, S., j. X. Zhao, Holasek, R. E., Torres, R., and King, A. J.: The Atmospheric Impact of the 1991 Mount Pinatubo Eruption, Quezon City : Philippine Institute of Volcanology and Seismology ; Seattle : University of Washington Press, http://pubs.usgs.gov/pinatubo/self/index.html, 1996.

Sigl, M., Winstrup, M., McConnell, J., Welten, K., Plunkett, G., Ludlow, F., Buentgen, U., Caffee, M., Chellman, N., Dahl-Jensen, D., Fischer, H., Kipfstuhl, S., Kostick, C., Maselli, O., Mekhaldi, F., Mulvaney, R., Muscheler, R., Pasteris, D., Pilcher, J., Salzer, M., Schuepbach, S., Steffensen, J., Vinther, B., and Woodruff, T.: Timing and climate forcing of volcanic eruptions for the past 2,500 years, Nature, 523, 543–549, doi:10.1038/nature14565, 2015.

Solomon, S.: Stratospheric ozone depletion: A review of concepts and history, Reviews of Geophysics, 37, 275–316, doi:10.1029/1999RG900008, http://dx.doi.org/10.1029/1999RG900008, 1999.

Staniforth, A. and Cote, J.: Semi-Lagrangian Integration Scheme for Atmospheric Models - A Review, Monthly Weather Review, 119, 2206–2223, 1990.

Stein, A. F., Draxler, R. R., Rolph, G. D., Stunder, B. J. B., Cohen, M. D., and Ngan, F.: NOAA's HYSPLIT Atmospheric Transport and Dispersion Modeling System, Bulletin of the American Meteorological Society, 96, 2059–2077, doi:10.1175/BAMS-D-14-00110.1, http://dx.doi.org/10.1175/BAMS-D-14-00110.1, 2015.

Wiesner, M. G., Wang, Y., and Zheng, L.: Fallout of volcanic ash to the deep South China Sea induced by the 1991 eruption of Mount Pinatubo (Philippines), Geology, 23, 885 – 888, 1995.

Wilson, L. and Huang, T.: The influence of shape on the atmospheric settling velocity of volcanic ash particles, Earth and Planetary Science Letters, 44, 311 – 324, 1979.

Wolfe, E. W. and Hoblitt, R. P.: Overview of the Eruptions, pp. 3–20, Quezon City : Philippine Institute of Volcanology and Seismology ; Seattle : University of Washington Press, http://pubs.usgs.gov/pinatubo/wolfe/index.html, 1996.